



Published in final edited form as:

Nat Immunol. 2020 October ; 21(10): 1181–1193. doi:10.1038/s41590-020-0753-y.

Basophils prime group 2 innate lymphoid cells for neuropeptide-mediated inhibition

Juan M. Inclan-Rico^{1,2}, John J. Ponessa^{1,2}, Nuriban Valero-Pacheco^{1,3}, Christina M. Hernandez^{1,2}, Chandler B. Sy^{1,2}, Alexander D. Lemenze⁴, Aimee M. Beaulieu^{1,3}, Mark C. Siracusa^{1,2}

¹Center for Immunity and Inflammation, New Jersey Medical School, Rutgers-The State University of New Jersey, Newark, New Jersey, USA

²Department of Medicine, New Jersey Medical School, Rutgers-The State University of New Jersey, Newark, New Jersey, USA

³Department of Microbiology, Biochemistry, and Molecular Genetics, New Jersey Medical School, Rutgers-The State University of New Jersey, Newark, New Jersey, USA

⁴Department of Pathology, Immunology and Laboratory Medicine, New Jersey Medical School, Rutgers-The State University of New Jersey, Newark, New Jersey, USA

Abstract

Type 2 cytokine responses promote parasitic immunity and initiate tissue repair but, can also result in immunopathologies when not properly restricted. Basophilia is recognized as a common feature of type 2 inflammation, however, the roles basophils play in regulating these responses remain unknown. Here, we demonstrate that helminth-induced ILC2 responses are exaggerated in the absence of basophils, resulting in increased inflammation and diminished lung function. Additionally, we show that ILC2s from basophil-depleted mice express reduced amounts of the receptor for the neuropeptide, neuromedin B (NMB). Critically, NMB stimulation inhibited ILC2 responses from control but not basophil-depleted mice, and basophils were sufficient to directly enhance NMB receptor (NMBR) expression on ILC2s. These studies suggest that basophils prime ILC2s to respond to neuron-derived signals necessary to maintain tissue integrity. Further, these data provide mechanistic insight into the functions of basophils and identify NMB as a potent inhibitor of type 2 inflammation.

Users may view, print, copy, and download text and data-mine the content in such documents, for the purposes of academic research, subject always to the full Conditions of use:http://www.nature.com/authors/editorial_policies/license.html#terms

Correspondence should be addressed to: Mark C. Siracusa, Department of Medicine, Rutgers New Jersey Medical School, Newark, NJ, mark.siracusa@rutgers.edu.

Author Contributions

J.M.I.R., J.J.P., N.V.P., C.M.H., C.B.S., A.D.L., and M.C.S. designed and performed the research. A.M.B. contributed to experimental design and data analysis, conceptualization, and manuscript editing. J.M.I.R. and M.C.S. analyzed experimental data and wrote the paper.

Competing Interests Statement

Mark C. Siracusa is the founder and president of NemaGen Discoveries.

Introduction:

The World Health Organization estimates that helminth infections affect approximately 2 billion people worldwide, causing malnutrition, growth impairment, cognitive deficiencies, and chronic immunopathology^{1,2}. Although antihelminthic drugs are available, they have short-lived effects, resulting in high reinfection rates within months of treatment³. Further, the generation of long-lasting immunotherapeutics has been precluded by our incomplete understanding of the mechanisms that properly regulate type 2 cytokine responses and host protection⁴. Therefore, developing a better understanding of the immunologic mechanisms that promote and/or inhibit type 2 inflammation would greatly inform the generation of new strategies to treat helminth infections and their associated morbidities.

Many helminths, such as hookworms, undertake complex migratory cycles that require their passage through multiple mucosal sites, including the lungs and gut. The passage of these large multicellular parasites is known to result in substantial wounding and tissue damage^{5,6}. In response to these signals, it is well-established that the mammalian host mounts potent type 2 cytokine responses, characterized by the secretion of interleukin (IL)-4, IL-5, and IL-13, which simultaneously promote parasite expulsion and the healing of affected tissues⁷. When properly regulated, type 2 cytokine responses are limited in order to reduce the detrimental effects of prolonged tissue remodeling and fibrosis⁸. The importance of balancing both resistance and tolerance mechanisms is evident by the severe chronic immunopathologies that can result if anti-helminth immunity is not properly regulated^{8,9}.

Elevated numbers of basophils in the periphery is a highly conserved characteristic of type 2 cytokine responses^{10,11}. Although basophils are known to secrete robust amounts of IL-4 upon activation, basophils are also capable of producing several soluble mediators including cytokines (IL-6, TNF, and IL-13), inflammatory molecules (histamine and platelet-activating factor), bioactive lipids (prostaglandins and leukotrienes), as well as growth factors (amphiregulin and CSF-1)^{10,11}. Given their capacity to secrete these potent effector molecules, it is not surprising that basophils are reported to operate as important mediators of allergic inflammation¹²⁻¹⁴. However, recent work has also begun to highlight the critical contributions of basophils during homeostatic conditions. For example, recent studies have demonstrated that basophils imprint on alveolar macrophages and play important roles during lung development, suggesting that the functions of basophils are context-dependent and extend beyond their ability to promote inflammation^{15,16}.

Consistent with their functional diversity in response to distinct stimuli, the roles basophils play in the context of antihelminth immunity appear to be parasite-specific. While studies have demonstrated that basophils promote type 2 inflammation and worm expulsion following *Trichuris muris* and *Trichinella spiralis* infections, their functions following other helminth infections remain unknown¹⁷⁻¹⁹. Although the population expansion of basophils in response to the hookworm *Nippostrongylus brasiliensis* (Nb) has been appreciated for several decades, the functions of Nb-induced basophils remain poorly understood. Further, important studies have demonstrated that depleting basophils following a primary Nb infection has no effect on worm clearance^{20,21}. These data suggest that Nb-induced basophils perform important functions that have yet to be appreciated.

A growing body of evidence has demonstrated that specialized innate immune cells engage in cellular cross-talk and cooperate to initiate type 2 inflammation^{6,22}. For example, basophils can promote the activation of group 2 innate lymphoid cells (ILC2s) via their secretion of IL-4^{12,14}. Additionally, recent reports show that neuron-derived signals such as neuromedin U (NMU) and calcitonin gene-related peptide (CGRP) are also capable of regulating the activation of ILC2s and thereby dictating the intensity of type 2 inflammation^{23–27}. Collectively, these studies suggest that intra-communication (immune cell to immune cell) and extra-communication (immune cell to neuron) might cooperate to direct the scope of type 2 responses. Despite these advances, whether immune cell-cross talk is required to facilitate subsequent neuroimmune interactions remains to be defined.

Here, we report that Nb-induced basophils accumulate in the lungs following the exit of parasitic larvae from the tissue, suggesting that they might contribute to host protection by promoting the healing of helminth-affected tissues rather than directly acting on the parasites. Consistent with this hypothesis, our data demonstrate that Nb-induced ILC2 responses are exaggerated in the absence of basophils, resulting in increased inflammation and reduced pulmonary function. Critically, overactive ILC2s from basophil-depleted mice exhibited reduced expression of the receptor for neuromedin B (NMB), a member of the neuromedin family of neuropeptides that include neuromedin B, C, K, L, N, U, and S^{28,29}. Importantly, treatment with exogenous NMB was sufficient to significantly reduce ILC2 responses, eosinophilia, and mucus production following Nb infection. Finally, while recombinant (r)NMB treatment inhibited sort-purified ILC2s from control mice, ILC2s from basophil-depleted mice were unresponsive to NMB stimulation, suggesting that basophils prime ILC2s for NMB-mediated inhibition. Altogether, our data highlight a previously unappreciated regulatory role for basophils in the context of antihelminth immunity and identify NMB as a potent inhibitor of type 2 inflammation.

Results:

Depletion of basophils results in severe helminth-induced pathology and impaired lung function.

Despite basophilia being a hallmark of type 2 inflammation^{10,11}, the roles these enigmatic cells play in regulating type 2 cytokine responses remain controversial^{20,21}. Therefore, we sought to better determine the functions of these rare immune cells following infection with the gastrointestinal nematode, *Nippostrongylus brasiliensis* (Nb). First, we evaluated several parameters of type 2 cytokine-mediated inflammation induced by Nb in the presence or absence of basophils. Lineage-specific depletion of basophils was achieved by administration of diphtheria toxin to Mcpt8^{tm1(cre)}LksyROSA26iDTR mice, as previously described²¹. While depletion did not alter inflammation in the gastrointestinal tract (Extended Data Fig. 1a) or worm expulsion (Fig. 1a), basophil depletion resulted in significantly increased type 2 cytokine responses in the lung (Fig. 1b), where the parasites transiently reside as part of their developmental life cycle. *In vivo* staining protocols used to distinguish blood-circulating versus tissue-resident cells revealed that tissue-resident basophil populations increased in the lungs starting on day 3 and peaked on day 5 post-infection (Fig. 1c, d). While effector cells activated in the context of type

2 cytokine responses are required to promote parasite clearance, they are also important for maintaining the integrity of parasite-affected tissues^{7,22}. Since Nb larvae exit the lung tissue on day 3 post-infection, before the majority of basophils are present, it is possible that basophils are playing a role in regulating inflammation in an attempt to restore lung function rather than serving to limit parasitic burdens. In support of this hypothesis, Nb-infected mice depleted of basophils exhibited altered lung pathology, marked by increased mucus production (Extended Data Fig. 1b, c), inflammatory cell infiltrates (Fig. 1e, Extended Data Fig. 1d) and had significantly reduced oxygen levels compared to control mice (Fig. 1f). Collectively, these data provoke the hypothesis that basophils limit infection-induced type 2 cytokine responses and assist in maintaining lung function post-Nb infection.

Basophil depletion results in elevated ILC2 responses

Microscopic analysis of lung pathology suggested that basophil-depleted mice had elevated infection-induced eosinophil responses. Flow cytometric analysis of bronchoalveolar lavage (BAL) fluid and lung infiltrates confirmed that while infection-induced neutrophilia was not significantly altered (Fig. 2a), (Extended Data Fig. 2a), basophil-depleted mice exhibited significantly increased BAL and lung eosinophil responses (Fig. 2b), (Extended Data Fig. 2b), as defined by flow cytometric gating strategies (Extended Data Fig. 2c). Nb-induced eosinophil responses and mucus production are dependent on IL-5 and IL-13, which are produced by ILC2s or CD4⁺ T cells^{6,7}. Lung basophil responses occur in the first few days post-infection (day 3–5), during the innate window when Nb-induced inflammation is reported to be ILC2-dependent^{6,22}. Further, the ability of basophils to communicate with and alter the activation state of ILC2s has been previously demonstrated^{12,14}. Therefore, we sought to determine if basophil-depleted animals exhibited elevated infection-induced ILC2 responses that correlated with increased mucus production and eosinophilia. Interestingly, ILC2 populations were increased in both the BAL and lung tissue of basophil-depleted mice compared to controls (Fig. 2c), (Extended Data Fig. 2d). Further, increases in IL-5 and IL-13 producing ILC2s were also detected (Fig. 2d, e), (Extended Data Fig. 2e, f), as defined by specific gating strategies (Extended Data Fig. 2g). Similar results were also observed in the BAL and lungs of infected *Mcpt8Cre* mice that constitutively lack basophils²⁰ (Extended Data Fig. 3a-f). However, despite increased IL-5 and IL-13 production by lung ILC2s, no increases in infection-induced eosinophil responses were observed in the lungs of *Mcpt8Cre* mice (Extended Data Fig. 3f). This is likely due to compensation mechanisms that are thought to exist in this constitutive mouse model¹¹. Importantly, basophil depletion in naïve mice did not alter ILC2 responses, suggesting that the observed differences are not due to diphtheria toxin receptor (DTR)-mediated cell death (Fig. 2c-e, Extended Data Fig. 2d-f). Nonetheless, to further rule out the possibility of off-target depletion effects, we next took a gain-of-function approach and transferred DTR negative basophils into basophil-depleted mice. Critically, the intratracheal transfer of DTR negative basophils was sufficient to suppress ILC2 responses, mucus production, and eosinophilia back to normal levels in both the BAL and lungs of basophil-depleted mice (Fig. 2f-i), (Extended Data Fig. 4a-g). Collectively, these loss- and gain-of-function approaches suggest that basophils negatively regulate lung ILC2 responses following a Nb infection.

Helminth-activated ILC2s exhibit reduced neuromedin B receptor expression in the absence of basophils

To further examine whether the effects of basophil depletion were occurring independently of adaptive lymphocytes, recombination-activating gene 2 (*Rag2*)-deficient mice were treated with the basophil-depleting antibody Ba103³⁰. *Rag2*^{-/-} mice treated with Ba103 exhibited significantly elevated Nb-induced ILC2 responses and eosinophilia in both the BAL (Fig. 3a, b) and lung (Fig. 3c, d). Further, *Rag2*^{-/-} mice treated with Ba103 also exhibited significantly elevated mucus production and altered lung pathology (Fig. 3e-f). Similar results were observed when basophils were depleted by treatment with the FcεRIα-specific antibody MAR-1¹⁹ (Extended Data Fig. 5a-f). Collectively, these data suggest that basophils negatively regulate lung ILC2 responses independently of adaptive lymphocytes. To elucidate the mechanism through which basophils regulate ILC2s, we first examined whether basophil depletion resulted in increased production of cytokine alarmins such as IL-25, IL-33, and TSLP, which promote ILC2 activation³¹. Importantly, no changes in the expression of *Il25* or *Tslp* were observed in the lungs of basophil-depleted mice. However, basophil-depleted mice exhibited significantly reduced expression of *Il33* in whole lung tissue (Extended Data Fig. 6a-c). Consistent with these data, analysis of IL-33-GFP reporter mice revealed that type 1 and type 2 pneumocytes expressed significantly less Nb-induced *Il33* following treatment with the anti-FcεRIα targeting antibody MAR-1 (Extended Data Fig. 6d, e). In aggregate, these studies suggest that elevated ILC2 responses in the basophil-depleted mice are not a result of increased cytokine/alarmin production. We next evaluated whether basophils suppress ILC2 activation via regulating mediators including anti-inflammatory cytokines, such as IL-10, or growth factors, like amphiregulin. Although no significant changes in *Il10* expression were detected in basophil-depleted mice, expression of amphiregulin was found to be significantly elevated in the absence of basophils (Extended Data Fig. 6f, g). Further, while basophils secreted robust amounts of activation-induced IL-6, we were unable to find detectable levels of basophil-derived IL-10 or amphiregulin (Extended Data Fig. 6h-j). Collectively, these data suggest that basophils are not regulating lung inflammation by producing these regulatory factors or amplifying their expression levels. Next, we performed single-cell RNA sequencing analysis to evaluate if the depletion of basophils substantially altered the composition of ILC2 populations. Single-cell RNA sequencing of lung-resident ILC2s revealed the presence of 6 distinct cell clusters defined by specific marker genes using the Seurat workflow (Extended Data Fig. 7a, b). Importantly, while basophil depletion did not result in substantial changes to the composition of ILC2s, helminth-induced expression of *Il5*, *Il13*, and *Areg* were significantly elevated across clusters of ILC2s sort-purified from basophil-depleted mice compared to control samples (Extended Data Fig. 7c). However, we did not detect significant changes in the expression of *Il1rl1* and *Arg1*.

While single-cell RNA sequencing is helpful to identify general differences across samples, the depth of gene lists can make it difficult to perform pathways analysis³². To address this, we also performed conventional RNA-sequencing of lung ILC2s post-Nb, to better identify how basophils may regulate their state of activation. Control ILC2s expressed a substantial number of genes at significantly higher levels than those from basophil-depleted mice (Fig. 4a, Extended Data Fig. 8a), (Supplementary table 1). Interestingly, pathway analysis

revealed that ILC2s from control animals were enriched for pathways including neuroactive ligand-receptor interactions, seven-pass-transmembrane domain receptor (7TM), G-protein-coupled receptor signaling, and rhodopsin-like signaling compared to ILC2s sort-purified from basophil-depleted mice (Fig. 4b). Notably, all three of these pathways are associated with neurotransmitter signaling, which has recently been identified as an important component of ILC2 activation post-Nb infection^{23–27}. Specifically, the neuropeptide, neuromedin U (NMU) produced by cholinergic neurons promotes ILC2 activation post-Nb^{23,24}. Importantly, NMU is part of the neuromedin family of neuropeptides including B, C, K, L, N, S, and U²⁹. Similar to NMU, neuromedin B (NMB) is expressed in the central nervous system, lungs, gastrointestinal tract, and adipose tissues of mammals^{28,29}. Further, both NMU and NMB signal through receptors belonging to the rhodopsin-like subfamily A7 of G-coupled protein receptors^{28,29}, which was identified by pathway analysis. While no significant changes in the receptors for NMU (NMUR1) or NMB (NMBR) were identified by RNA-sequencing analysis on day 5 post-infection, when ILC2s were sort-purified from the lungs of mice on day 7 post-Nb (following the peak of lung basophilia), significant reductions in *Nmbr* expression were observed in basophil-deficient animals (Fig. 4c). Further, while surface expression of NMBR by ILC2s was increased post-infection, ILC2s from basophil-depleted mice exhibited significantly reduced surface levels of NMBR protein (Fig. 4d, e). Interestingly, NMBR expression in alveolar macrophages was not altered when basophils were depleted (Fig. 4f), suggesting that basophils regulate NMBR expression in a cell-specific manner. Notably, expression of *Nmu* and *Nmb* ligand in the lung remained unchanged following basophil depletion (Fig. 4g). Collectively, these data provoke the hypothesis that basophils regulate ILC2 responses by altering their ability to respond to NMB-mediated signals.

Neuromedin B is a potent inhibitor of Nb-induced type 2 cytokine responses

To investigate if NMB operates as a negative regulator of type 2 cytokine responses, wild-type mice were infected with Nb and treated with rNMB. On day 7 post-infection, parameters of type 2 cytokine-dependent inflammation were evaluated in both the BAL and lung. Strikingly, rNMB-treated wild-type mice exhibited reduced ILC2 responses and eosinophilia in both compartments (Fig. 5a-f). Further, rNMB treated mice also showed increased disruption of the alveoli, significantly reduced mucus production, and failed to clear worms as efficiently as control mice (Fig. 5g-j). Collectively, this gain-of-function approach further suggests that NMB operates as a potent inhibitor of type 2 inflammation.

While NMB is reported to regulate cell growth, body temperature, blood pressure, and glucose levels via its effects on non-hematopoietic cells, its ability to alter the activation state of immune cells remains unknown²⁹. To address this, we first evaluated expression of NMBR by CD45⁺ immune cells and found that NMBR is expressed by ILC2s, CD4⁺ T cells, alveolar macrophages, non-alveolar macrophages and eosinophils (Extended Data Fig. 8b-f). Collectively, these data suggest that NMB may influence Nb-induced inflammation via its effects on several cells of hematopoietic origin. To further evaluate whether NMB-NMBR signaling is important in the hematopoietic compartment, we generated NMBR-floxed mice (Extended Data Fig. 9a) and crossed them with Vav-iCre mice to remove NMBR expression from CD45-expressing cells³³. As expected, NMBR was significantly

reduced on CD45⁺ cells, including ILC2s, but remained unchanged in the non-hematopoietic compartment (Fig. 6a-c). Similar to basophil depletion, NMBR^{fl/fl} x Vav-iCre⁺ mice exhibited significantly increased expression of *Il4*, *Il5* and *Il13* in lungs on day 7 post-Nb infection (Extended Data Fig. 9b-d). Critically, NMBR^{fl/fl} x Vav-iCre⁺ mice also presented with significantly elevated cytokine responses by ILC2s and elevated eosinophilia in both the BAL (Fig. 6d-h) and lungs (Extended Data Fig. 9e-g) post-Nb. Additionally, selectively targeting NMBR expression in the hematopoietic compartment also resulted in significantly elevated *Muc5ac* expression and increased cellular infiltrates in the lung (Fig. 6i, j). Collectively, these data suggest that NMB-NMBR signaling on immune cells is required to properly regulate Nb-induced inflammation.

Neuromedin B is a potent inhibitor of innate immunity to Nb

The data above suggest that basophils regulate NMB-NMBR-signaling that is required to limit type 2 cytokine responses post-Nb. Further, these studies suggest that NMB may act on cells in both the innate and adaptive immune compartments. Nb-induced basophils enter the lungs between days 3–7 post-infection (Fig. 1d) when type 2 cytokine responses are reported to be primarily ILC2 driven^{6,22}. Therefore, we sought to determine if NMB can negatively regulate Nb-induced inflammation independently of adaptive lymphocytes. To test this, *Rag2*^{-/-} mice were infected with Nb and treated with rNMB. Consistent with experiments in wild-type mice, *Rag2*^{-/-} mice treated with rNMB exhibited significantly reduced ILC2 and eosinophil responses in both the BAL and lung (Fig. 7a-c), (Extended Data Fig. 9h-k). Further, rNMB-treated *Rag2*^{-/-} mice also exhibited significantly reduced mucus production and impaired worm expulsion, suggesting that rNMB treatment is sufficient to inhibit type 2 inflammation in the absence of adaptive lymphocytes (Fig. 7d, e). rNMB-treated *Rag2*^{-/-} mice also presented with significantly elevated expression of *Il17* and increased neutrophilia, suggesting that in the absence of type 2 cytokine production, early Nb-induced IL-17 responses remain elevated^{34,35} (Fig. 7f-g, Extended Data Fig. 9l). Finally, rNMB treatment resulted in severe lung pathology and significantly elevated numbers of red blood cells in the BAL, an indication of a reduced capacity to initiate type 2-dependent wound healing^{36,37} (Fig. 7h-j). Collectively, these data suggest that NMB operates as a potent negative regulator of innate type 2 responses.

Neuromedin B directly inhibits ILC2s

The above studies demonstrate that NMBR is expressed by several innate cell populations known to promote anti-helminth immunity. Further, gain-of-function studies demonstrate that rNMB is sufficient to inhibit Nb-induced ILCs responses *in vivo*. However, whether NMB acts directly on ILC2s remains unknown. To test this, we sort-purified lung ILC2s from Nb-infected control and basophil-depleted mice and cultured them *in vitro* for 24 h. This allowed us to remove the cells from the inhibitory presence of the NMB ligand. In the absence of NMB ligand, ILC2s from control and basophil-depleted mice produced similar amounts of IL-5 and IL-13 (Fig. 8a). However, addition of rNMB significantly reduced production of IL-5 and IL-13 by ILC2s from control mice, but had no impact on cytokine production by ILC2s obtained from basophil-depleted animals (Fig. 8a). Importantly, WT ILC2s treated with rNMB showed increased survival, suggesting that reduced cytokine levels were not a result of increased cell death (Fig. 8b). Similar results were also seen

when WT ILC2s were sort-purified and stimulated with IL-33 and NMB simultaneously (Extended Data Fig. 10a-d). These data illustrate that NMB directly alters the activation state of ILC2s and suggest that basophils regulate this process.

The above data suggest that basophils prime ILC2s for NMB-mediated inhibition via their ability to regulate NMBR expression. However, whether basophils regulate NMBR expression in a direct or indirect manner remains unknown. To address this, we co-cultured ILC2s either alone or in the presence of activated basophils and monitored surface expression of NMBR as well as cytokine secretion and cell proliferation. As previously reported^{14,15}, co-culture of ILC2s with activated basophils resulted in elevated secretion of cytokines but failed to promote changes in ILC2 proliferation (Extended Data Fig. 10e-g). Critically, ILC2s co-cultured with basophils also exhibited significantly increased surface expression of NMBR (Fig. 8c, d). Importantly, the ability of basophils to promote receptor expression was not a conserved feature of ILC2 activation, as IL-33 treatment had no effect on NMBR levels (Fig. 8e). Basophils are known to produce several important effector molecules including cytokines and lipid mediators that are capable of influencing the activation state of distinct immune cells including ILC2s^{12,14,38,39}. Therefore, we also tested if the basophil-associated effector molecules IL-4 and prostaglandin E2 (PGE₂) are sufficient to increase NMBR expression. While IL-4 was found to have no effect, PGE₂ stimulation resulted in significantly increased surface expression of NMBR by sort-purified ILC2s (Fig. 8e). Collectively, these data suggest that basophils might prime ILC2s for NMB-mediated inhibition, in part, through their expression of PGE₂.

Prostaglandin E2 and NMB cooperate to inhibit ILC2 activation

While, no changes in ILC2 viability were observed following NMB stimulation (Fig. 8b), it is possible that NMB inhibits ILC2s via its effect on cell proliferation and/or cytokine production. To evaluate whether rNMB affects proliferation, we stained sort-purified ILC2s with CellTrace™ Violet (CTV) and monitored cell division by employing a previously described culture system⁴⁰. As expected, ILC2s showed strong proliferative capacity with approximately 40% of the cells undergoing 2–3 divisions and 15% of the cells undergoing 4–5 divisions over the 4-day culture period. As a positive control for inhibition, cultures were treated with PGE₂⁴¹. Consistent with previous reports, PGE₂ stimulation resulted in significantly decreased percentages of cells achieving between 2–5 divisions (Fig. 8f,g). Importantly, rNMB treatment alone showed no effect on the proliferation of ILC2s (Fig. 8f,g). Given the ability of PGE₂ to restrict ILC2 proliferation and our data demonstrating that PGE₂ appears to prime ILC2s for NMB-mediated inhibition (Fig. 8e), we sought to test if the two signals cooperate to simultaneously restrict both ILC2 proliferation and cytokine production. Similar to our previous data, ILC2s cultured with PGE₂ showed significantly increased expression of NMBR in our proliferation assays (Fig. 8h). Further, when PGE₂ and NMB were added together significantly less IL-5 and IL-13 were detected in culture supernatants, suggesting that the two signals cooperate to inhibit ILC2s via combined effects on proliferation and cytokine production (Fig. 8i).

While our data demonstrate that NMB-NMBR signaling inhibits ILC2 cytokine production, the molecular pathways that promote these changes remain to be defined. Therefore, we

stimulated sort-purified ILC2s with either PBS or rNMB and performed RNA-sequencing analysis. Following rNMB stimulation, ILC2s exhibited significantly downregulated expression of the P2x purinoceptor 7 (*P2rx7*) a gene previously linked to ILC2 activation⁴² (Fig. 8j, Extended Data Fig. 10h, i) (Supplementary table 2). To evaluate if P2rx7 inhibition phenocopies the effects of NMB treatment we treated sort-purified ILC2s with the P2rx7 inhibitor brilliant blue G⁴² and monitored IL-5 and IL-13 levels. Consistent with the effects of rNMB treatment, inhibition of P2rx7 resulted in significantly reduced levels of IL-5 and IL-13 (Fig. 8k). Collectively, these data suggest that NMB may restrict ILC2 cytokine production via its inhibition of P2rx7.

Discussion

The findings presented above identify a previously unappreciated aspect of cross-talk between basophils and ILC2s. Moreover, these data suggest that communication between innate immune cells is required to promote neuro-immune interactions, necessary to maintain tissue integrity. While it is well-appreciated that robust type 2 cytokine production is vital to promote host protective responses to helminths^{5,6}, our understanding of how this inflammation is restricted to prevent persistent tissue remodeling remains understudied. The data presented here identify a complex cellular and molecular network that is required to properly inhibit helminth-induced inflammation and identify a role for basophils in regulating these events.

While basophils have long been associated with type 2 cytokine-mediated inflammation, their diverse cellular functions have remained largely underappreciated. Although the dramatic basophilia that occurs following a Nb infection has been recognized for over 40 years^{43,44}, the functions of Nb-elicited basophils remain controversial. Although several studies have reported that basophils are not required to promote Nb expulsion^{20,21}, our data indicate that basophils enter the lungs after the parasitic larvae exit the tissue, suggesting that basophils are likely to participate in promoting tissue homeostasis. Interestingly, recent studies have also determined that basophils infiltrate the lung during tissue development, where they serve important functions by programming alveolar macrophages^{15,16}. Our data suggest that basophils might perform regenerative functions following an inflammatory response, in order to promote tissue homeostasis. A similar role for eosinophils in the lung has recently been established⁴⁵, suggesting that type 2-associated granulocytes may perform tissue-protective functions in some contexts.

It is well established that communication between several innate immune populations is required to initiate potent type 2 cytokine responses. For example, basophils have been reported to activate ILC2s via their secretion of IL-4^{12,14}. In response to these signals, ILC2s secrete vast amounts of IL-5 and IL-13 that elicit several events, such as eosinophil recruitment and mucus production by goblet cells. Nonetheless, whether innate immune cells also communicate to efficiently limit type 2 inflammation and prevent chronic tissue remodeling is not well understood. The studies presented here highlight a novel interaction between basophils and ILC2s that allows them to receive inhibitory signals induced by the neuropeptide NMB. It is possible that in the process of activating ILC2s via IL-4 secretion, basophils also prime ILC2s to receive regulatory signals required to limit the duration of

their activation. This concept may be similar to the effects observed during T cell activation, in which TCR stimulation results in the induction of the inhibitory molecules PD-1 and CTLA-4 that become important negative regulators after the initial activation phase is completed^{46,47}. Importantly, basophils, but not IL-4, were sufficient to induce NMBR on ILC2s, further supporting the notion that additional signaling pathways are initiated when basophils interact with ILC2s.

PGE₂ is a well-defined lipid mediator known to be released by activated basophils³⁸. Importantly, our data demonstrate that PGE₂ is sufficient to induce the expression of NMBR on ILC2s, although to a lesser extent than basophils. Interestingly, PGE₂ can inhibit ILC2 proliferation⁴¹ and our data show that NMB selectively targets ILC2 cytokine production. Therefore, our data suggest a model where NMB and PGE₂ might cooperate to suppress ILC2 activation via their combined effects of proliferation and cytokine production. A similar concept is proposed by Nagashima *et al.*²⁷ where the neuropeptide CGRP shaped ILC2 functions by limiting NMU-induced proliferation and IL-13 secretion while supporting IL-5 production, suggesting that ILC2s may be regulated in specific manners that tailor to optimal outcomes. Although further studies are required to fully define the molecular actions of NMB, our data suggest that it might operate via its ability to regulate P2rx7 expression.

A growing body of evidence has demonstrated that highly coordinated interactions between the nervous and immune system are required to initiate host-protective responses against helminths⁴⁸. However, whether similar communication events exist to limit helminth-induced inflammation remain to be fully defined. This is perhaps most evident in the context of ILC2 biology, where numerous mediators of activation, including NMU^{23,24}, VIP⁴⁹, and serotonin⁵⁰, have been identified compared to a relatively limited number of inhibitors. Importantly, our studies identify a novel regulatory pathway in which NMB suppresses cytokine secretion by ILC2s, with basophils operating as the transition switch required for ILC2s to respond to NMB-mediated inhibition. Critically, our studies have also identified the expression of NMBR in several immune cells, including CD4⁺ T cells and alveolar macrophages, highlighting the need to further evaluate this critical pathway in other model systems. In summary, these data provide insight into the highly coordinated cellular and molecular events needed to allow for the necessary initiation, but carefully regulated persistence, of type 2 inflammation in the lung.

Materials and Methods

Mice

8–10 week old C57BL(6) wild type (WT) (stock #000664), Mcpt8^{tm1(cre)Lksy} (stock #017578)²¹, ROSA26iDTR (stock #007900), Rag2^{-/-} mice (stock #008449), IL-33^{fl/fl}-eGFP mice⁵¹ (stock #030619), and Vav-iCre mice³³ (stock #008610) were purchased from The Jackson Laboratory. Mcpt8Cre-4get²⁰ mice were kindly provided by Dr. David Voehringer. Lineage-specific depletion of basophils was obtained by crossing Mcpt8^{tm1(cre)Lksy} mice with ROSA26iDTR mice as previously described^{21,52}.

NMBR-floxed mice were generated by Cyagen Biosciences Inc. Briefly, the gRNA to mouse Nmbr gene, the donor vector containing loxP sites flanking exon 2 of the Nmbr gene, and

Cas9 mRNA were co-injected into fertilized mouse eggs to generate targeted conditional knockout mice. F0 founder animals were identified by PCR followed by sequence analysis. Positive offspring were then bred to wild type mice to test germline transmission and F1 animal generation. F1 mice were bred with wild type mice to generate more positive F2 animals, which were identified by PCR. NMBR floxed hemizygous mice were bred to generate homozygous offspring, which were then crossed with Vav-iCre hemizygous mice to target NMBR expression specifically on all hematopoietic cells. NMBR floxed homozygous Vav-iCre negative littermates were used as control.

All mice were maintained in specific pathogen-free facilities at the Rutgers New Jersey Medical School. All protocols were approved by the Rutgers Institutional Animal Care and Use Committee (IACUC), Protocol number 00968.

N. brasiliensis infection and pharmacologic treatments

Methods for maintenance, recovery, infection and isolation of *Nippostrongylus brasiliensis* (Nb) larvae were performed as previously described⁵³. Mice were infected with 500 Nb larvae by subcutaneous injection. For basophil depletion, WT and basophil-depleted mice were treated with 0.375 μ g of diphtheria toxin (LIST biological laboratories, Cat. #150) i.p. every other day; mice were sacrificed 3–7 days post-Nb infection. Intestinal worm burdens were evaluated 7 days post-infection as described previously⁵³. For neuromedin B treatment, mice were anesthetized with isoflurane and then treated with 10 μ g of neuromedin B (MP Biomedicals) dissolved in 50 μ L of PBS administered via intratracheal instillation. For antibody-mediated basophil depletion, Rag2^{-/-} mice were treated with 20 μ g of anti-Fc ϵ RI (antibody (clone MAR-1, eBioscience) or anti-CD200R3 antibody (clone Ba103, Hycult Biotech) i.p. on days 1, 3, and 5 post-Nb infection.

Basophil transfer

WT mice were injected intravenously (i.v.) with a combination of 1 μ g mouse recombinant IL-3 (R&D systems) and 0.5 μ g of α -IL-3 antibody (BioLegend: clone MP2–8F8) in 200 μ L of PBS 3 days prior to euthanasia as previously described⁵⁴. At necropsy, single cell suspensions of spleens were prepared and basophil populations were sort-purified as described below using a FACSAriaII (BD Bioscience). Purity for all cell populations were determined to be 98% or greater. Then, 15,000 basophils were resuspended in 50 μ L of PBS and transferred into each mouse via intratracheal instillation at days 3, 4, 5, and 6 after Nb infection.

Intravascular in vivo flow cytometry stain

Intravascular *in vivo* staining protocols were performed similar to previously described⁵⁵. Briefly, mice were injected intravenously with 3 μ g of the basophil-specific fluorescent-labeled antibody anti-CD200R1 (clone OX110, eBioscience) diluted in 300 μ L of PBS, 5 minutes prior to euthanasia. Then, basophil populations in the lung tissue were analyzed by flow cytometry.

Preparation of lung and bronchioalveolar lavage (BAL) cell suspensions

For BAL collection after necropsy, 3–5 mL of PBS were injected and aspirated from the trachea of each mouse, and the volume of BAL obtained was recorded. Following BAL collection, lungs were collected at necropsy and single-cell suspensions for flow cytometric analysis were prepared as previously described⁵⁶. Briefly, pulmonary tissue was minced and incubated in HBSS containing 2.5% of FBS, collagenase D (2 mg/mL, Roche) and DNase I (80 U/mL, Roche) for 30 min at 37°C. Cell suspensions were then filtered through a 100µm filter and analyzed by flow cytometry. Additionally sections of pulmonary tissue were collected for real-time PCR and histological analysis.

Flow cytometry and cell sorting

Cells were stained with monoclonal anti-mouse fluorescently conjugated antibodies: B220 (RA3–6B2), CD3 (145–2C11), CD4 (GK1.5), CD5 (53–73), CD19 (1D3), NK1.1 (PK136), CD11b (MI/70), CD11c (N418), IgE (23G3), FcεRI α (MAR-1), CD31 (MEC 13.3), CD49b (DX5), CD45 (30-F11), CD64 (X54–5/7.1), CD90 (5E10), CD127 (A7R34), CD200R1 (OX110), CD200R3 (Ba13), EpCAM (G8.8), F4/80 (BM8), $\gamma\delta$ TCR (eBioGL3), Siglec-F (E50–2440), Ly6G (1A8), Ly6C (AL-21), IL-5 (TRFK5), IL-13 (eBio13A), PDPN (8.1.1), Ter-119 (TER-119) from eBioscience or BD Biosciences. For intracellular staining, cells were incubated for 5 hours at 37°C with Leukocyte Activation Cocktail, with BD GolgiPlug™ (BD Biosciences) following manufacturer's instructions. For NMBR staining rabbit anti-mouse NMBR antibody (NLS825) was used from Novus Biologicals at 10µg/mL. Basophils were analyzed as CD45⁺CD3⁻CD19⁻NK1.1⁻Ly6G⁻Siglec-F⁻CD200R3⁺CD49b⁺CD200R1⁺FcεRI α ⁺. Eosinophils were analyzed as CD45⁺CD11b⁺Siglec-F⁺CD11c⁻. Neutrophils were evaluated as CD45⁺CD11b⁺Ly6G⁺. ILC2s were identified as CD45⁺CD3⁻CD19⁻CD11b⁻CD11c⁻NK1.1⁻B220⁻CD5⁻Ter-119⁻ $\gamma\delta$ TCR⁻FcεR⁻CD90⁺CD127⁺IL-5⁺IL-13⁺. Alveolar macrophages were analyzed as CD45⁺F4/80⁺CD64⁺Siglec-F⁺CD11c⁺. Non-alveolar macrophages were analyzed as CD45⁺F4/80⁺CD64⁺Siglec-F⁻CD11c⁺. CD4 T cells were defined as CD45⁺CD3⁺CD90⁺CD4⁺. Type 1 pneumocytes were evaluated as CD45⁻Ter-119⁻CD31⁻EpCAM⁺PDPN⁺. Type 2 pneumocytes were identified as CD45⁻Ter-119⁻CD31⁻EpCAM⁺PDPN⁻. Samples were acquired on a BD Fortessa flow cytometer (BD Biosciences) and analyzed using FlowJo software (v10.0.5, Tree Star). Cell sorting was performed using a FACS Aria II (BD Bioscience).

ILC2 in vitro cultures

Lung cells were isolated from WT or basophil-depleted mice infected with Nb 7 days prior. Then, ILC2 populations (CD45⁺Lin⁻CD90⁺CD127⁺) were sorted and 10,000 cells were cultured in the presence of 10 ng/mL of mouse recombinant IL-2, IL-7 (R&D systems), and vehicle (PBS) or 1 µg/mL of Neuromedin B for 20–24 hours. For some experiments, 10ng/mL of mouse recombinant IL-33, IL-4 (R&D systems), 100nM of Prostaglandin E₂ (PGE₂) (Cayman chemicals), or 1µM of brilliant blue G (Sigma-Aldrich) were added to ILC2 cultures. Cell viability was evaluated by 7-AAD (Biolegend Cat #420403) and Annexin V (Biolegend Cat #640920) double negative staining. Supernatant levels of IL-5 and IL-13 were then evaluated by ELISA. For intracellular staining, BD Golgi Plug™

Protein Transport Inhibitor (Cat. #555029) was added for the last 4 hours of incubation and cells were stained and analyzed as described above. NMBR expression was evaluated by flow cytometry analysis as indicated above.

For ILC2 basophil co-cultures, lung-resident ILC2 populations were sort-purified from WT or Rag2^{-/-} mice after 7 days of Nb infection and cultured with basophils sort-purified from WT mice injected with 1µg of mouse recombinant IL-3 3 days prior. ILC2s and basophils were co-cultured for 24 hours in the presence of mouse recombinant IL-2, IL-7, and IL-3 (10ng/mL).

ILC2 proliferation was evaluated as described previously⁴⁰. Briefly, 10,000 sort-purified lung-resident ILC2s were labeled with CellTrace™ Violet (CTV) (Thermo Fisher Scientific, Cat. #C34571) following manufacturer's protocol and cultured with 5,000 irradiated (1500 Rad) OP9-DL1 cells (kindly provided by Dr. Derek Sant'Angelo), in the presence of mouse recombinant IL-2 and IL-7 (10ng/mL). For some conditions, NMB (1 µg/mL), PGE₂ (100nM), or 10,000 sort-purified basophils were added. After 4 days of culture, CTV dilution was determined by flow cytometry.

RNA isolation and quantitative real-time PCR analysis

RNA from sections of lung tissue was isolated by homogenization in TRIzol (Invitrogen) followed by phenol-chloroform extraction and isopropanol precipitation. cDNA was generated per standard protocol with Superscript reverse transcriptase (Invitrogen) and used as input for real-time PCR. Real-time PCR data were analyzed using the CT method using SYBR Green chemistry (Applied Biosystems), with βNA serving as the endogenous housekeeping gene. All reactions were run on an ABI 7500 Fast Real-Time PCR System (Applied Biosystems). Samples were normalized to naïve controls. The following QuantiTech primer assays from Qiagen were used: Areg (QT00112217), IL-4 (QT00160678), IL-5 (QT00099715), IL-10 (QT00106169), IL-13 (QT00099554), IL-17a (QT00103278), IL-25 (QT00134645), IL-33 (QT00135170), Mcpt8 (QT00131565), Muc5ac (QT01161104), Nmb (QT00105945), Nmb1 (QT00312494), Nmu (QT00133091), Nmur1 (QT00174006), and Tslp (QT00198261).

Global and single cell RNA-sequencing

Lung-resident ILC2s from control and basophil-depleted mice were sort-purified on live CD45⁺CD3⁻CD19⁻CD11b⁻CD11c⁻NK1.1⁻B220⁻CD5⁻Ter-119⁻γδTCR⁻Fc γδRIα⁻CD90⁺CD127⁺ cells from three biological replicates and pooled. Purity for all cell populations were determined to be 98% or greater. For bulk RNA-sequencing, RNA was extracted using Qiagen RNeasy plus™ micro kit (Cat. #74034), and amplified using Ambion MessageAmp II aRNA™ Amplification Kit (Cat. #AM1751). Illumina compatible libraries were generated using the NEBNext Ultra II kit (NEB E7645S) and sequenced using an Illumina NextSeq 550 in a single end 75bp read configuration. Bulk RNA-sequencing analysis was performed in accordance with the NF-Core RNA-sequencing guidelines (version 1.4.2)⁵⁷. The output reads were aligned to the GRCm38 genome using STAR, followed by gene count generation using featureCounts and StringTie⁵⁸⁻⁶⁰. Read counts were normalized and compared for differential gene expression using DESeq2 with

significance at False Discovery Rate (FDR) adjusted p-value < 0.05 ⁶¹. For analysis of functional pathways, the Database for Annotation, Visualization, and Integrated Discovery (DAVID) platform⁶² was used.

For single-cell RNA-sequencing, 10,000 sort-purified ILC2s were processed using the 10X Genomics Chromium™ Controller. Cell suspensions were loaded onto the Chromium Single Cell A Chip for cell lysis and barcoding. RNA from individual cells was reverse transcribed and sequencing libraries prepared using the Chromium™ Single Cell 3' Library Kit v2, following the manufacturers protocol. Samples were sequenced using an Illumina NextSeq 550 with standard 10X Genomics Configuration (26bp \times 98bp). After sequencing, raw bcl files were processed using the cellranger mkfastq command for sample demultiplexing and conversion to .fastq files, followed by cellranger count for cell barcode and UMI deconvolution as well as mapping to the respective reference genome. Processed digital gene expression matrices were imported into R studio for analysis using the Seurat package. Samples were aligned along common sources of variation and compared using canonical correlation analysis to identify unique clusters of cells within the samples. Marker genes for each sample and cluster were identified and used for generation of downstream plots within the Seurat package. All packages are maintained to be best in class and are regularly updated to their most recent release.

Pulse oximetry

Oxygen saturation was evaluated with the MouseOx Plus® (Starr Lifesciences Corp) following manufacturer's instructions. Briefly, the hair around the thigh was removed 1 day before Nb infection. Then, mice were anesthetized with 5% isoflurane and oxygen saturation was monitored using the thigh sensor for an interval of approximately 5 minutes. This time point was used to collect representative and error-free data.

Histology

Lung sections were fixed in formalin 10% buffered for at least 3 days, followed by processing in a Leica ASP300 tissue processor following manufacturer's instructions. Tissue blocks were paraffin-embedded using a Leica EG1150H Embedding Module and then sliced into 5 μ m sections using a Leica RM2235 rotatory microtome. Tissue sections were then deparaffinized, hydrated and stained with hematoxylin & eosin (H&E) or periodic acid-Schiff (PAS) methods. Images were acquired with a Keyence BZ-X710 All-in-One fluorescence microscope (Keyence, Osaka, Japan) and analyzed using the Keyence BZ-X Viewer version 01.03 software.

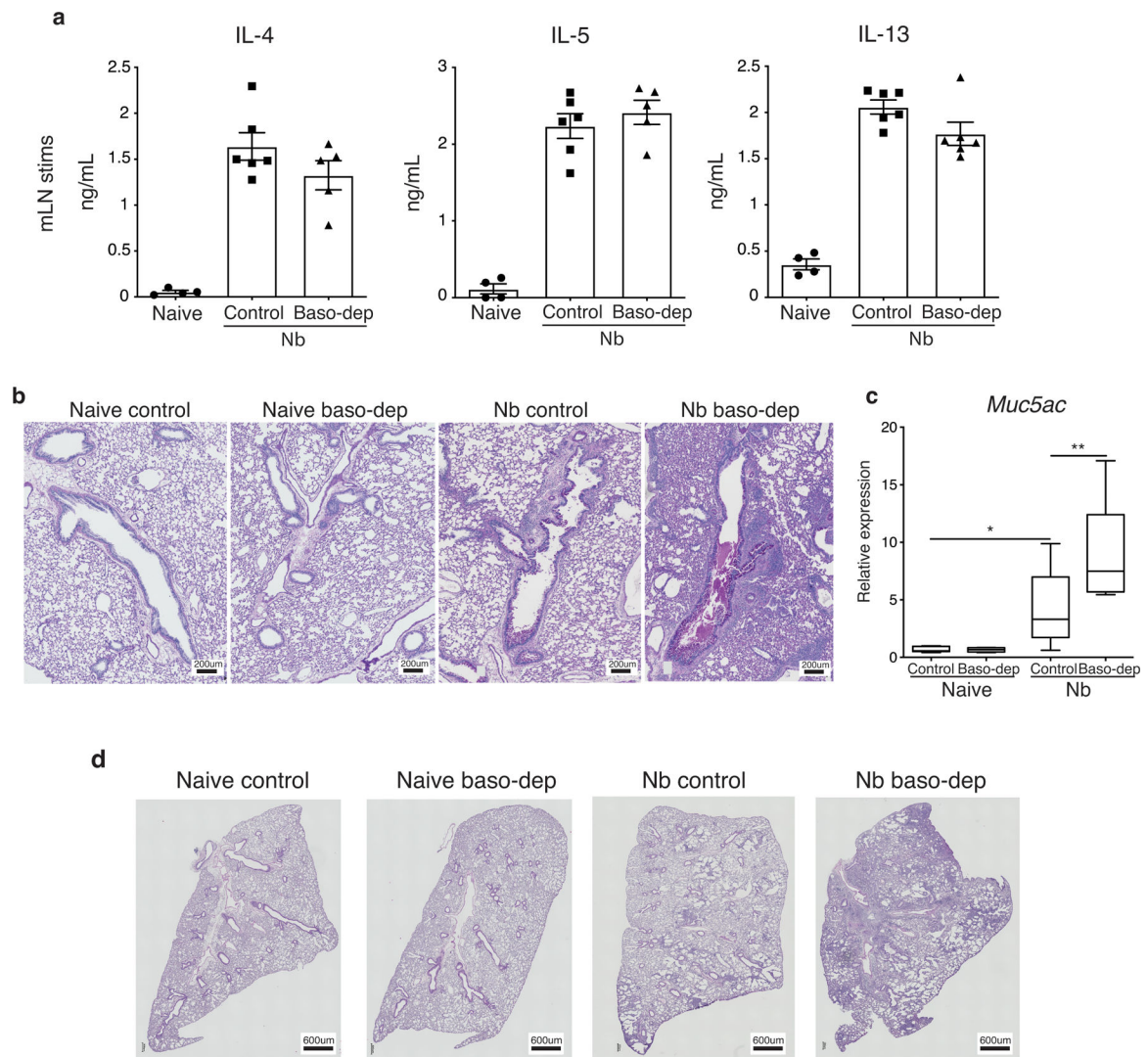
Statistics

Results are shown as mean \pm standard error of the mean. $P < 0.05$ was considered as significantly different. Statistical analysis was performed using Student's *t*-tests in GraphPad Prism version 8.

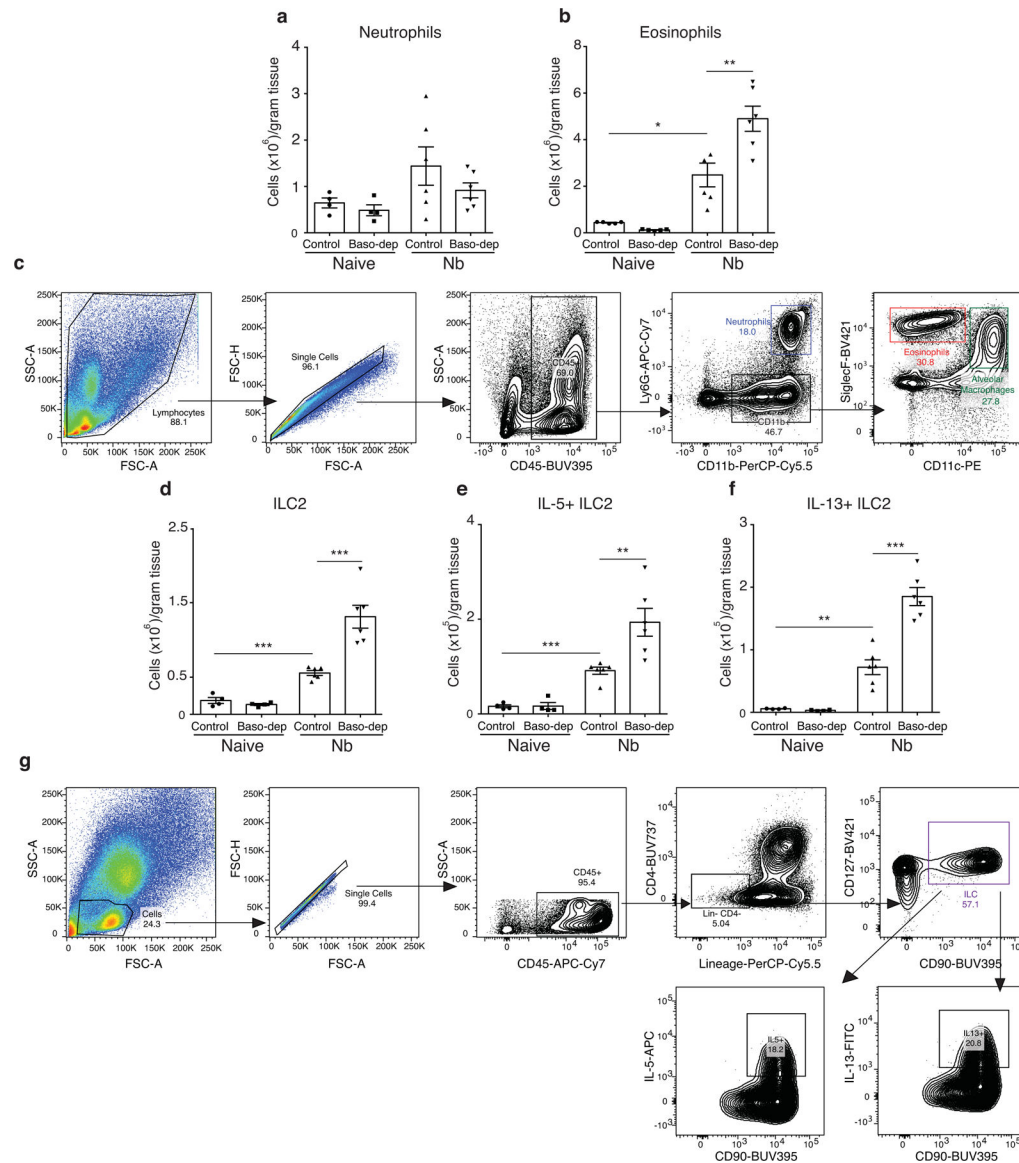
Reporting Summary.

Further information on research design is available in the Nature Research Life Sciences Reporting Summary linked to this article.

Extended Data

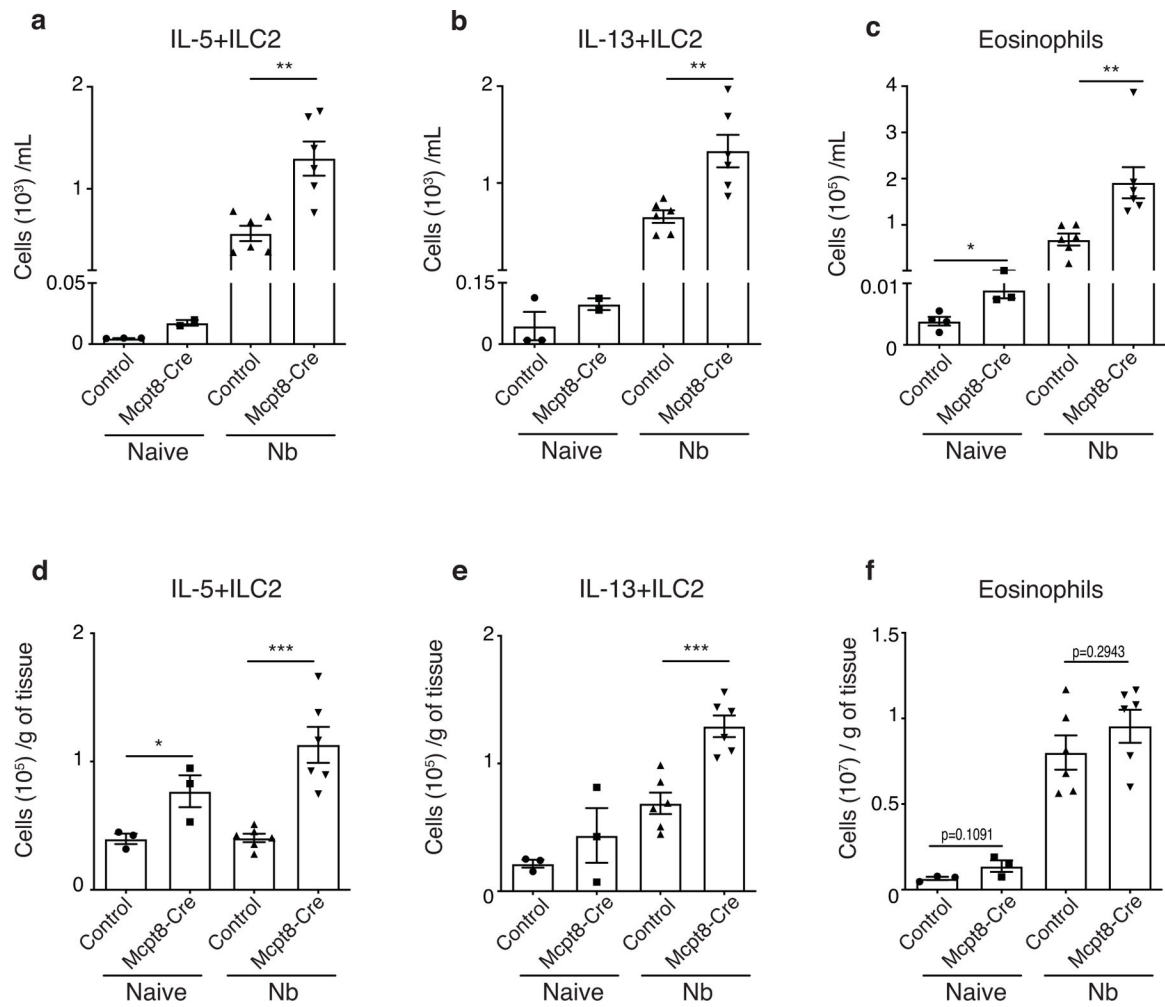
**Extended Data Figure 1. Basophils limit helminth-induced pulmonary inflammation.**

(a) Supernatant levels of IL-4, IL-5 and IL-13 from re-stimulated mesenteric lymph nodes (mLNs) isolated from control or basophil-depleted mice. Mucus production was evaluated in control and basophil-depleted mice on day 7 post-Nb infection by (b), periodic acid shiff (PAS) staining and (c), *Muc5ac* expression in the lungs by real-time PCR. (d), Lung pathology was evaluated by H&E-stained sections with individual images digitally tiled together to provide a larger overview. *P* values were determined by two-tailed Student's *t*-tests. (a-d), Representative of at least 3 separate experiments with at least 5 mice per group. **P* < 0.05, ***P* < 0.01, ****P* < 0.001. (b), Illustrate data pooled from 2 separate experiments.



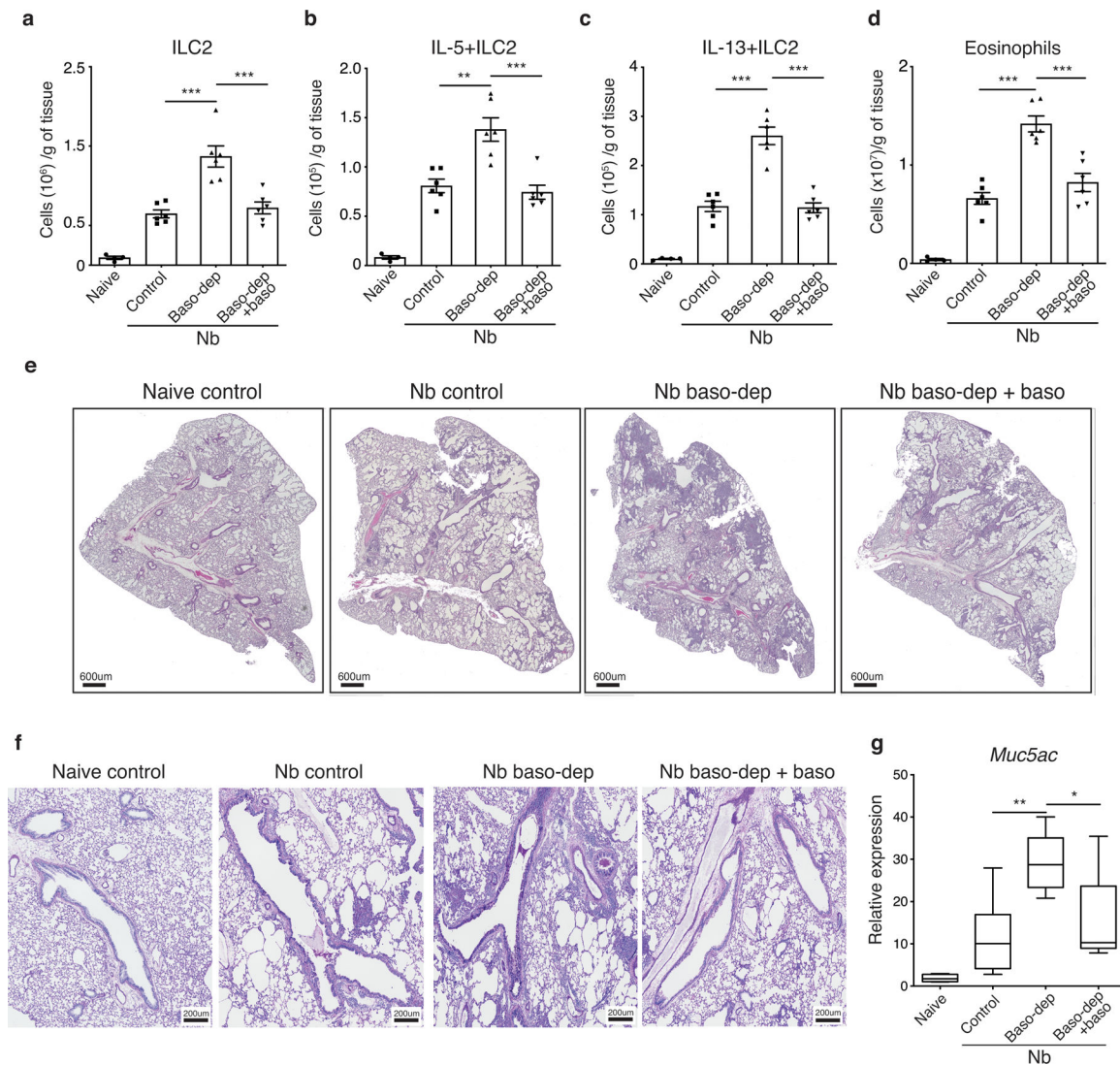
Extended Data Figure 2. Basophil depletion results in elevated ILC2 responses.

(a), Lung neutrophils and (b), eosinophils were quantified by flow cytometry on day 7 post-Nb infection in control or baso-dep mice. (c), Representative flow cytometric gating strategy to evaluate neutrophils and eosinophils. (d), ILC2s in the lung were quantified on day 7 post-Nb infection in control or baso-dep mice. Intracellular cytokine staining for (e, f), IL-5 and IL-13 was performed on lineage negative, CD90⁺, CD127⁺ ILC2s in lung on day 7 post-Nb infection and cytokine positive cells were quantified. (g), Representative flow cytometric gating strategy to evaluate ILC2 populations. *P* values were determined by two-tailed Student's *t*-tests. **P* < 0.05, ***P* < 0.01, ****P* < 0.001. (a-g), Representative of at least 3 separate experiments with at least 5 mice per group.

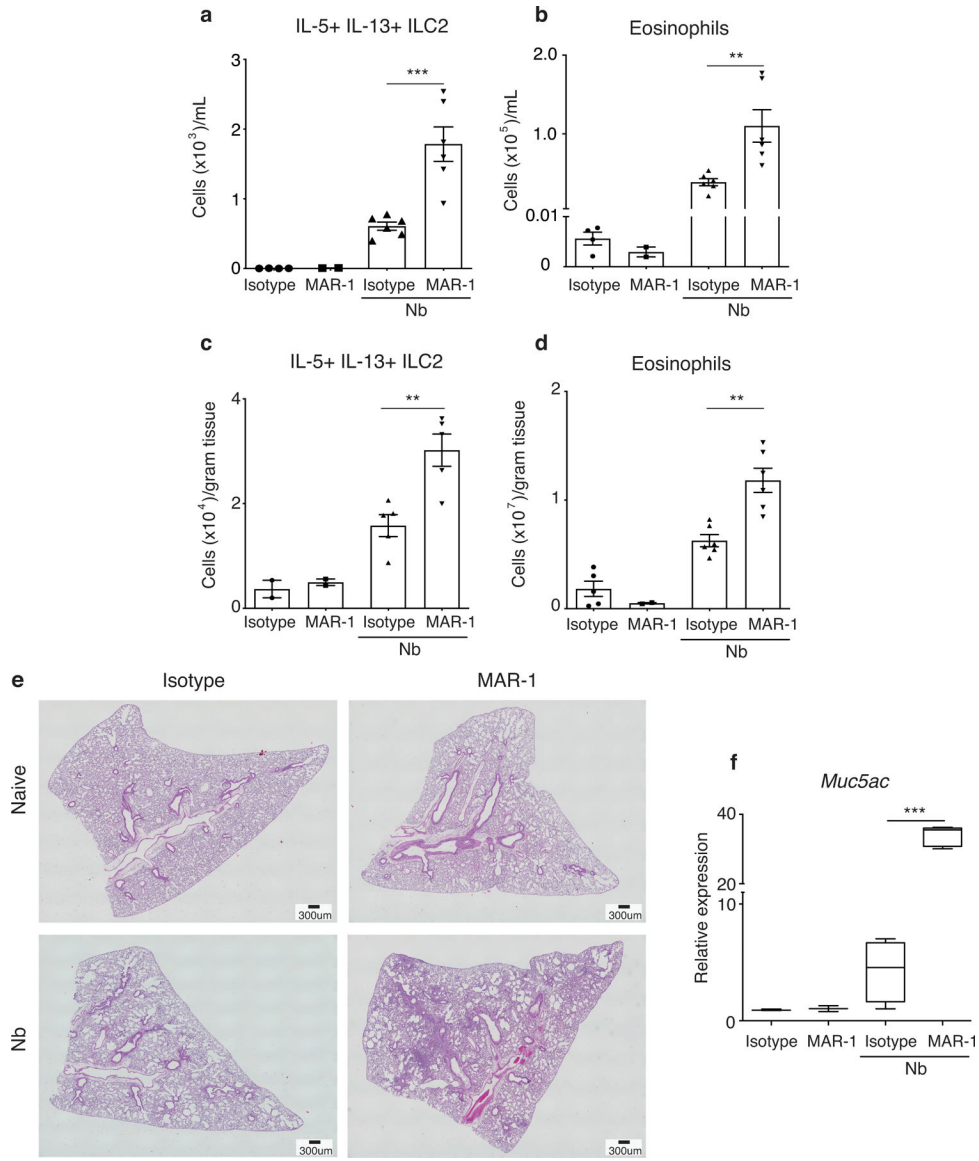


Extended Data Figure 3. Constitutive ablation of basophils is associated with increased ILC2 activation.

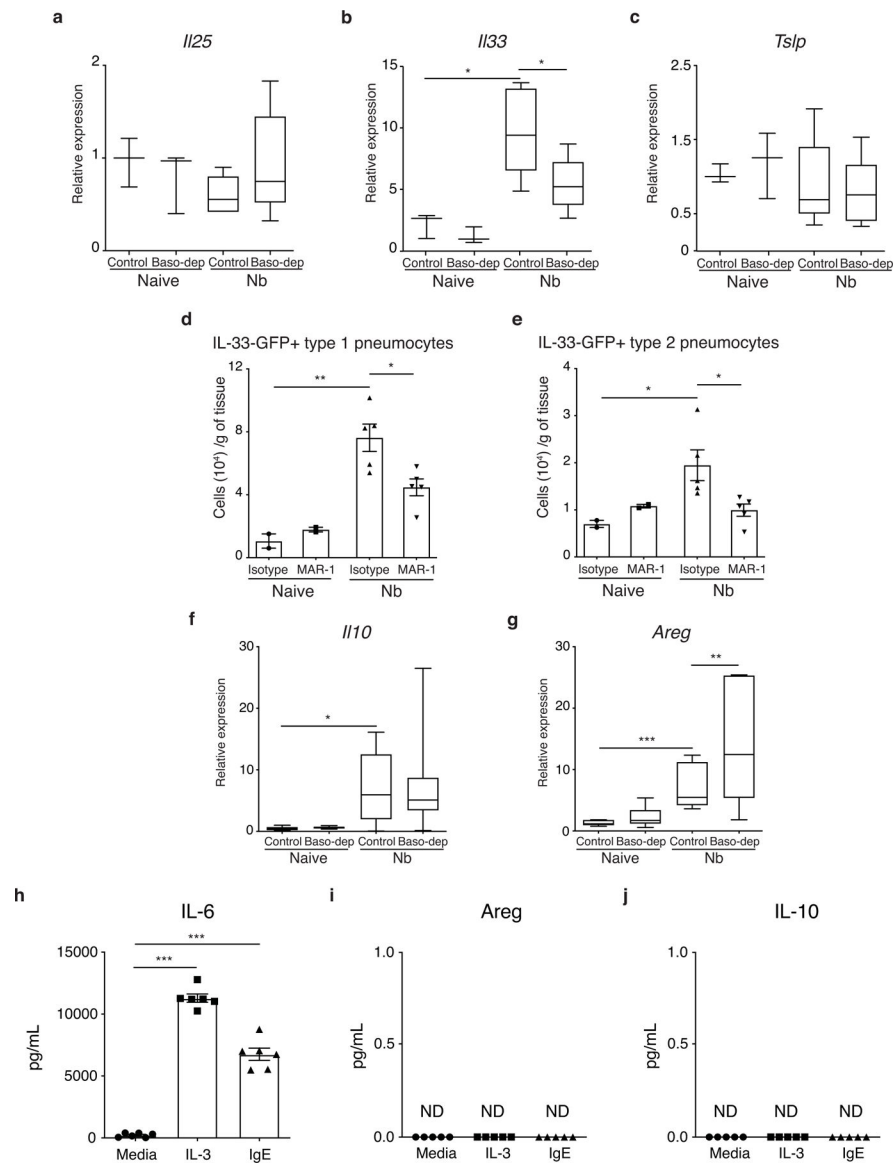
(a, b), IL-5+ and IL-13+ ILC2s, as well as (c), eosinophils in the BAL and (d-f), lungs were quantified in control and Mcpt8Cre-4get mice that constitutively lack basophils, 7 days post-Nb infection. *P* values were determined by two-tailed Student's *t*-tests. **P* < 0.05, ***P* < 0.01, ****P* < 0.001. (a-f), Representative of at least 3 separate experiments with at least 5 mice per group.



Extended Data Figure 4. Basophils are sufficient to limit helminth-induced ILC2 responses. (a), ILC2 numbers, (b), ILC2 production of IL-5, and (c), IL-13, as well as (d) eosinophil numbers were quantified in the lung on day 7 post-Nb infection in control mice, baso-dep mice, or baso-dep mice that received adoptive transfers of basophils. (e), H&E staining of lung sections on day 7 post-Nb infection with individual images digitally tiled together to provide a larger overview. Mucus production in the lung was evaluated by (f), PAS staining of lung sections and (g), *Muc5ac* expression. *P* values were determined by two-tailed Student's *t*-tests. **P* < 0.05, ***P* < 0.01, ****P* < 0.001. (a-g), Representative of at least 3 separate experiments with at least 4 mice per group.

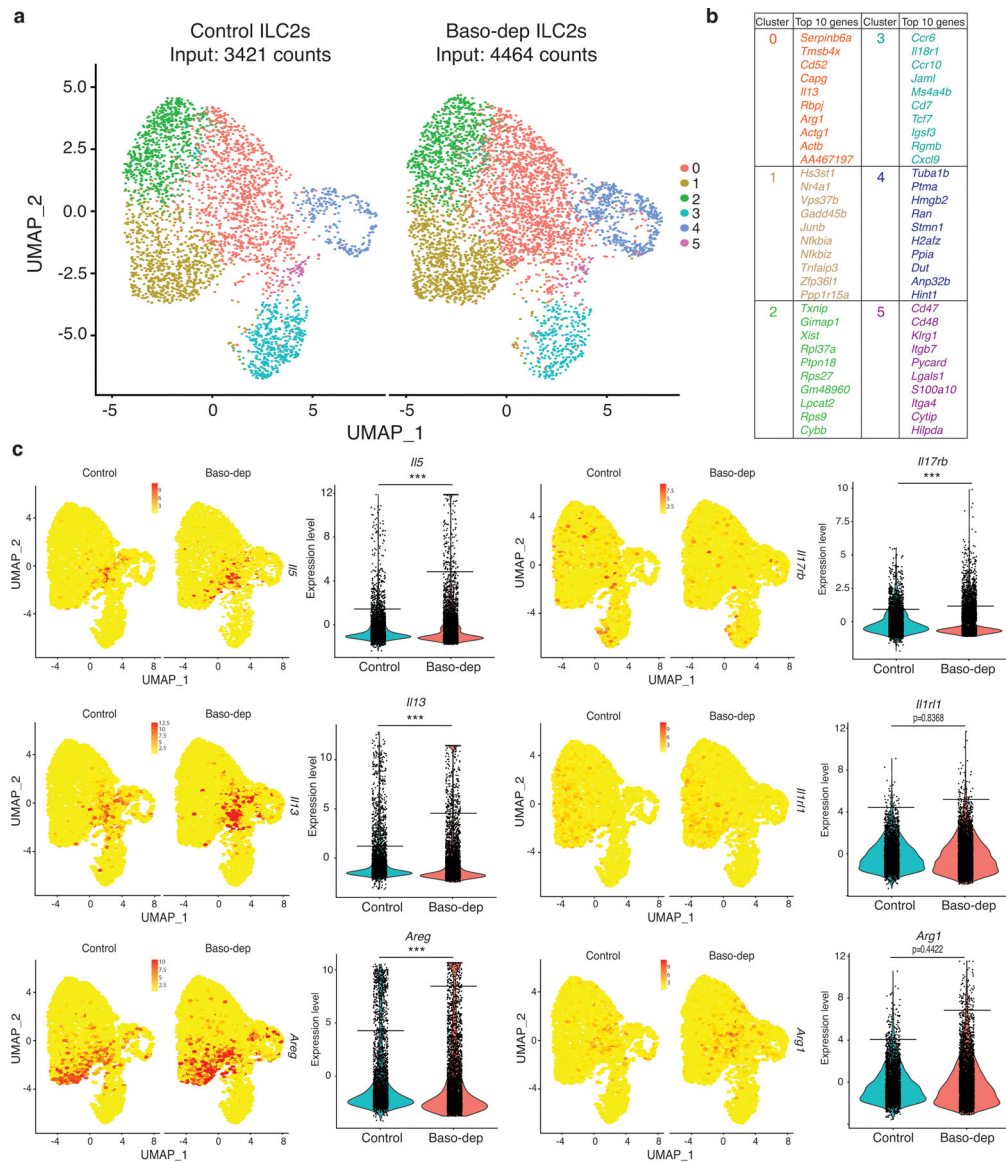


Extended Data Figure 5. Basophils regulate ILC2s independently of adaptive lymphocytes. Nb-infected *Rag2*^{-/-} mice were treated with isotype control or the basophil-depleting antibody MAR-1 and (a), ILC2 responses and (b), eosinophilia were determined in the BAL and (c,d), lung on day 7 post-infection. (e), H&E staining of lung sections on day 7 post-Nb infection with individual images digitally tiled together to provide a larger overview. (f), Mucus production in the lung was evaluated by *Muc5ac* expression. *P* values were determined by two-tailed Student's *t*-tests. **P* < 0.05, ***P* < 0.01, ****P* < 0.001. (a-f), Representative of at least 3 separate experiments with at least 2 mice per naive groups and at least 4 mice per infected groups.



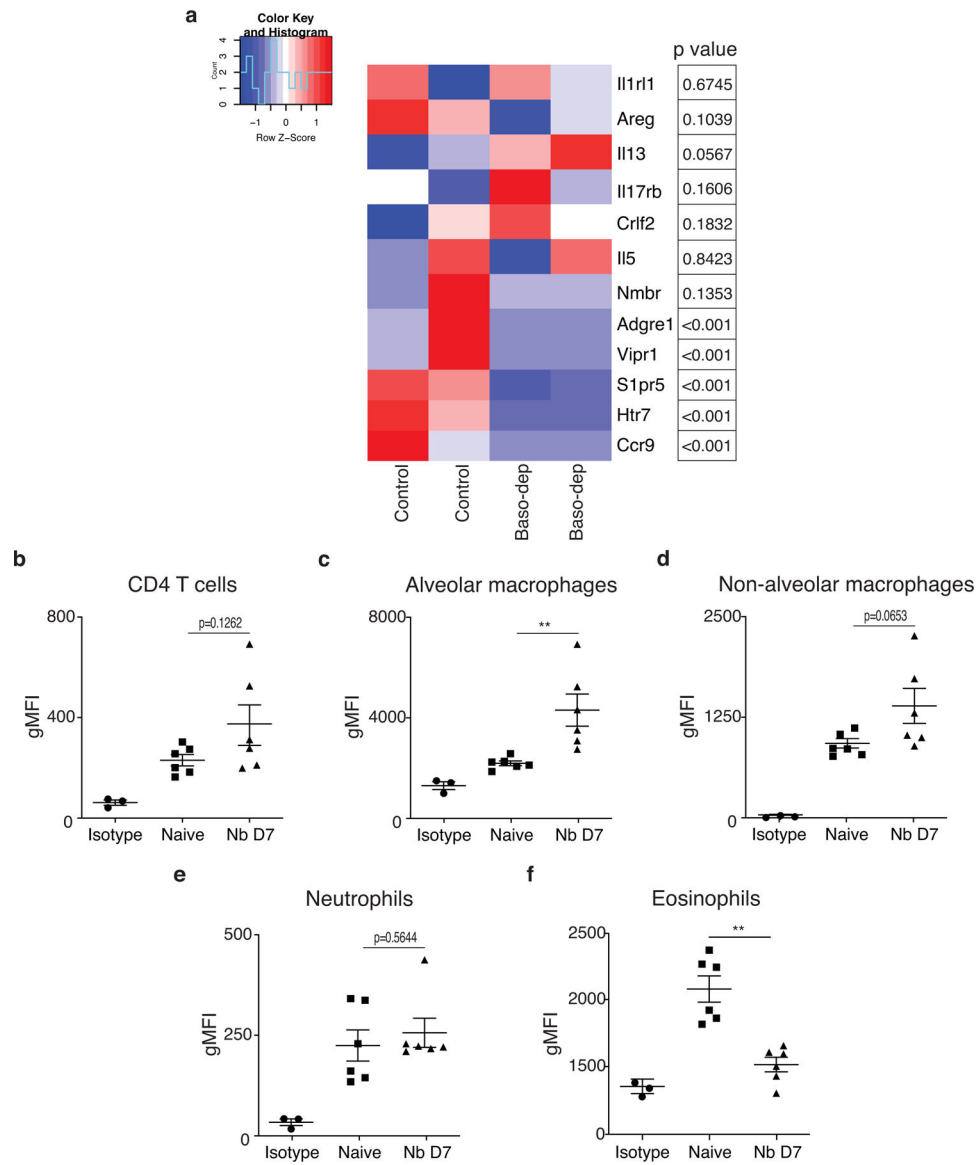
Extended Data Figure 6. Elevated ILC2 responses are not associated with increased cytokine alarmin expression.

(a-c), Expression of cytokine alarmins in the lungs of control and baso-dep mice was determined on day 7 post-Nb infection by real-time PCR. (d, e), Numbers of IL-33-GFP+ type 1 and type 2 pneumocytes were evaluated in IL-33-GFP-reporter mice infected with Nb and treated with the basophil-depleting antibody MAR-1. Expression of (f), *Il10* and (g), *Areg* in the lungs of control and baso-dep mice was determined on day 7 post-Nb infection by real-time PCR. Splenic basophils were sort-purified and cultured (O/N) with IL-3 and anti-IgE antibody and supernatant levels of (h), IL-6, (i), amphiregulin (Areg), and (j), IL-10 were evaluated by ELISA. *P* values were determined by two-tailed Student's *t*-tests. **P* < 0.05, ***P* < 0.01, ****P* < 0.001. (a-g), Representative of at least 2 separate experiments with at least 2 mice per naive groups and at least 5 mice per infected groups. (h-j) Representative of at least 3 separate experiments with at least 5 individual samples of sort-purified basophils from 5 mice per experimental group.

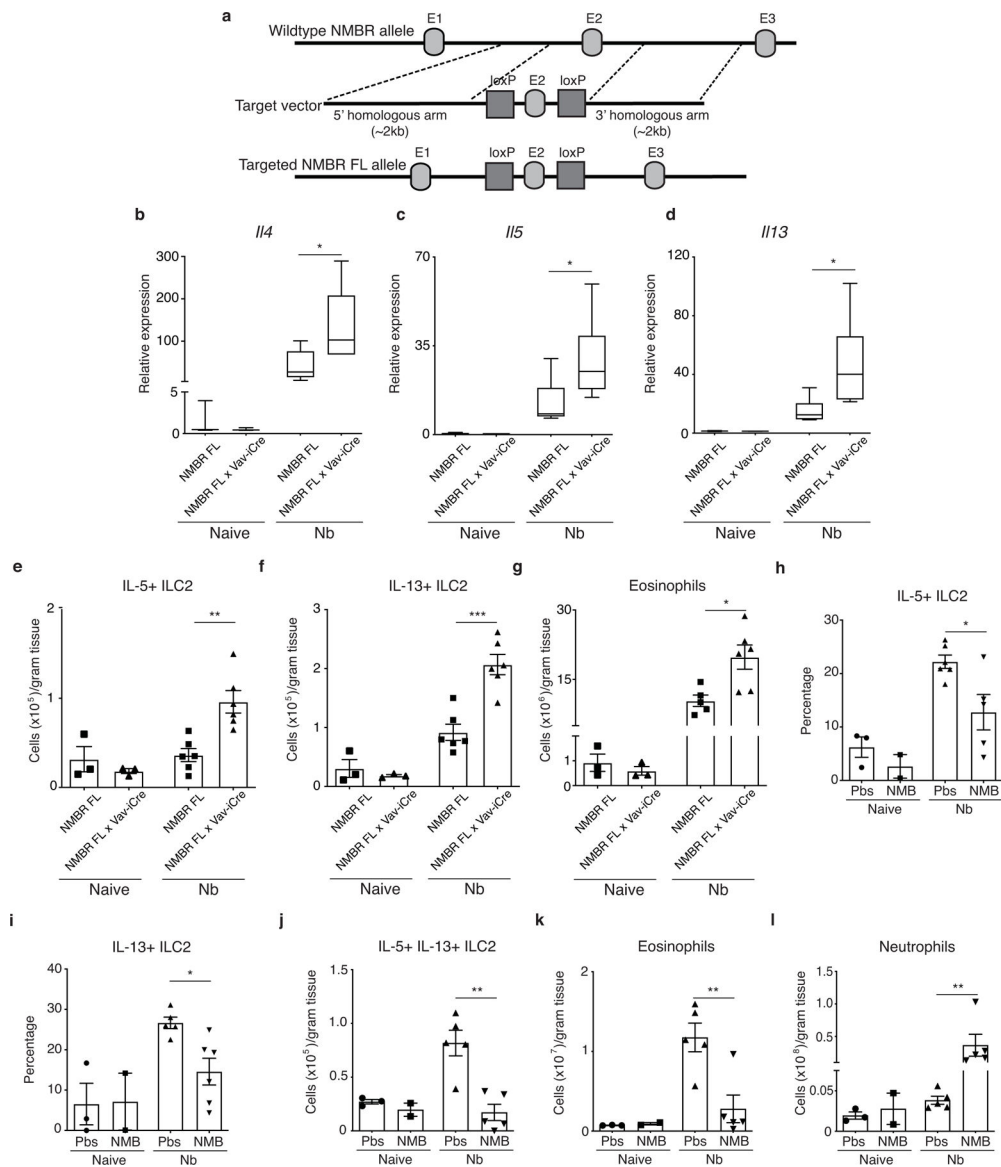


Extended Data Figure 7. Single cell RNaseq analysis of lung-resident ILC2s.

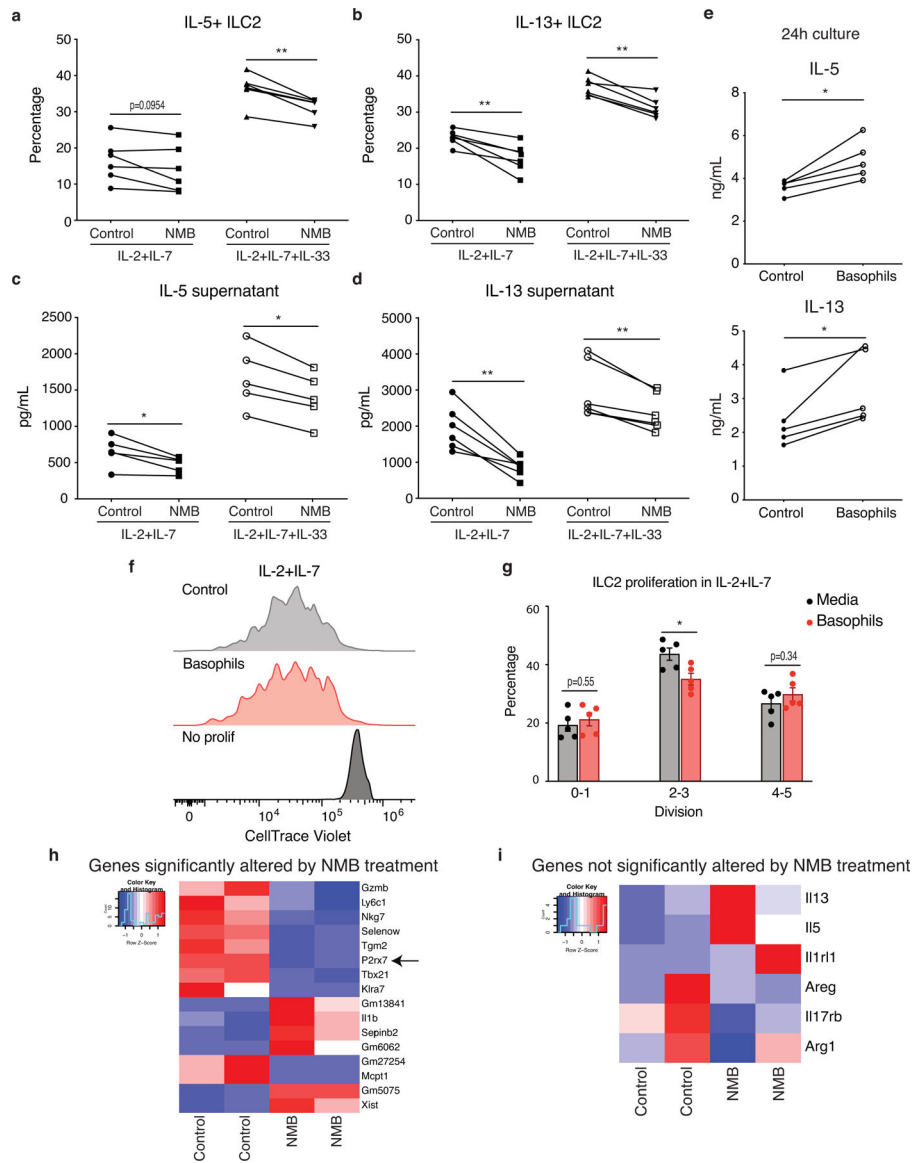
(a), Uniform Manifold Approximation and Projection (UMAP) plot illustrating defined clusters of cells generated by single cell RNA-sequencing of lung-resident live ILC2 populations ($CD45^+Lin^-CD90^+CD127^+$) sort-purified from control (and basophil-depleted (baso-dep) mice 5 days post-Nb infection. (b), Top 10 marker genes expressed by each cluster of ILC2s. (c), Single-cell expression of *Il5*, *Il13*, *Arg*, *Arg1*, *Il1r1*, and *Il17rb* in ILC cell clusters as defined in A. Horizontal bars represent mean normalized expression. *P* values were determined by Wilcoxon signed rank sum test. * $P < 0.05$, ** $P < 0.01$, *** $P < 0.001$.



Extended Data Figure 8. Analysis of NMBR expression in the hematopoietic compartment. (a), Heat map illustrating representative genes of interest expressed in control or baso-dep ILC2s. Surface NMBR expression by (b), CD4⁺ T cells, (c), alveolar macrophages, (d), non-alveolar macrophages, (e), neutrophils, and (f), eosinophils was determined in lung suspensions of naïve and mice infected with Nb 7 days prior. *P* values were determined by two-tailed Student's *t*-tests. **P* < 0.05, ***P* < 0.01, ****P* < 0.001. (b-f), Representative of at least 3 separate experiments with at least 2 mice per naïve groups and at least 4 mice per infected groups.



Extended Data Figure 9. NMB-NMBR signaling suppresses helminth-induced ILC2 responses. (a), Schematic illustrating targeting strategy and placement of loxP cassettes upstream and downstream of exon 2 of the *Nmbr* gene. (b-d), Type 2 cytokine expression in the lungs of *NMBR^{fl/fl}* controls and *NMBR^{fl/fl} x Vav-iCre⁺* mice was determined on day 7 post-Nb infection by real-time PCR. (e), IL-5⁺ and (f), IL-13⁺ ILC2s, as well as (g), eosinophils were quantified in the lungs of *NMBR^{fl/fl} x Vav-iCre⁺* mice 7 days post-Nb. Nb-infected *Rag2^{-/-}* mice were treated with PBS or rNMB (i.t.) and (h, i), the percentage of IL-5⁺ and IL-13⁺ ILC2s were determined in the BAL and (j), the total number of IL-5⁺ and IL-13⁺ ILC2s were determined in the lung on day 7 post-infection. (k), eosinophils and (l), neutrophils were determined in the lungs of *Rag2^{-/-}* mice treated with PBS or rNMB on day 7-post infection. *P* values were determined by two-tailed Student's *t*-tests. **P* < 0.05, ***P* < 0.01, ****P* < 0.001. (b-l), Representative of 3 separate experiments with at least 3 mice per naive groups and at least 5 mice per infected groups.



Extended Data Figure 10. Basophils are required for NMBR-mediated inhibition of ILC2s. Sort-purified ILC2s were cultured (O/N) with vehicle or rNMB in the presence of IL-2 and IL-7 or IL-2, IL-7, and IL-33. **(a, b)**, The percentage of IL-5⁺ and IL-13⁺ ILC2s were quantified by intracellular staining. **(c, d)**, IL-5 and IL-13 levels in the supernatant were quantified by ELISA. Sort-purified ILC2s were cultured (O/N) alone or with activated basophils. **(e)**, Cytokine levels in the supernatant were monitored by ELISA and **(f, g)**, cell proliferation was evaluated by CTV dilution 4 days post-culture. **(h)**, Heat map illustrating genes differentially expressed at 2.0-fold or higher between control or NMB-treated ILC2s. **(i)**, Heat map illustrating genes not differentially expressed in control or NMB-treated ILC2s. *P* values were determined by two-tailed Student's *t*-tests. **P* < 0.05, ***P* < 0.01, ****P* < 0.001. (a-g) Representative of at least 3 separate experiments with at least 5 individual samples of sort-purified ILC2s in each experimental group.

Supplementary Material

Refer to Web version on PubMed Central for supplementary material.

Acknowledgments

We thank members of the Center for Immunity and Inflammation for discussions and critical reading, the NJMS Flow Cytometry and Immunology Core Laboratory for technical assistance, the NJMS Histology Core, and the NJMS Genomics Research Lab for bioinformatics assistance. We also thank Dr. David Voehringer for kindly providing the *Mcpt8Cre* mice and Dr. Derek Sant'Angelo for providing the OP9-DL1 cell line. This work was supported by the National Institutes of Health (RO1 AI123224 and RO1 AI131634 to M.C.S., T32AI125185 to C.B.S. and 3R01AI131634-02W1 to C.M.H.). J.M.I.R. is supported by the Mexican Council of Science & Technology (CONACyT, CVU 536876).

Data availability statement.

Bulk RNAseq and single cell RNAseq data is deposited in the GEO accession code GSE150793. Source data for all figures are provided with the manuscript.

References

- Schistosomiasis and soil-transmitted helminthiases: number of people treated in 2015. *Wkly Epidemiol Rec* 91, 585–595 (2016). [PubMed: 27934297]
- Jourdan PM, Lamberton PHL, Fenwick A & Addiss DG Soil-transmitted helminth infections. *Lancet*, doi:10.1016/S0140-6736(17)31930-X (2017).
- Jia TW, Melville S, Utzinger J, King CH & Zhou XN Soil-transmitted helminth reinfection after drug treatment: a systematic review and meta-analysis. *PLoS neglected tropical diseases* 6, e1621, doi:10.1371/journal.pntd.0001621 (2012). [PubMed: 22590656]
- Zhan B et al. Advancing a multivalent 'Pan-anthelmintic' vaccine against soil-transmitted nematode infections. *Expert Rev Vaccines* 13, 321–331, doi:10.1586/14760584.2014.872035 (2014). [PubMed: 24392641]
- Allen JE & Maizels RM Diversity and dialogue in immunity to helminths. *Nature reviews. Immunology* 11, 375–388, doi:10.1038/nri2992 (2011).
- Harris NL & Loke P n. Recent Advances in Type-2-Cell-Mediated Immunity: Insights from Helminth Infection. *Immunity* 47, 1024–1036, doi:10.1016/j.immuni.2017.11.015 (2017). [PubMed: 29262347]
- Gause WC, Wynn TA & Allen JE Type 2 immunity and wound healing: evolutionary refinement of adaptive immunity by helminths. *Nature reviews. Immunology* 13, 607–614, doi:10.1038/nri3476 (2013).
- Gieseck Iii RL, Wilson MS & Wynn TA Type 2 immunity in tissue repair and fibrosis. *Nature Reviews Immunology* 18, 62, doi:10.1038/nri.2017.90 (2017).
- Marsland BJ, Kurrer M, Reissmann R, Harris NL & Kopf M *Nippostrongylus brasiliensis* infection leads to the development of emphysema associated with the induction of alternatively activated macrophages. *Eur J Immunol* 38, 479–488, doi:10.1002/eji.200737827 (2008). [PubMed: 18203142]
- Sullivan BM & Locksley RM Basophils: a nonredundant contributor to host immunity. *Immunity* 30, 12–20, doi:10.1016/j.immuni.2008.12.006 (2009). [PubMed: 19144314]
- Voehringer D Protective and pathological roles of mast cells and basophils. *Nature reviews. Immunology* 13, 362–375, doi:10.1038/nri3427 (2013).
- Kim BS et al. Basophils promote innate lymphoid cell responses in inflamed skin. *Journal of immunology* 193, 3717–3725, doi:10.4049/jimmunol.1401307 (2014).
- Siracusa MC, Kim BS, Spergel JM & Artis D Basophils and allergic inflammation. *The Journal of allergy and clinical immunology* 132, 789–788, doi:10.1016/j.jaci.2013.07.046 (2013). [PubMed: 24075190]

14. Motomura Y et al. Basophil-derived interleukin-4 controls the function of natural helper cells, a member of ILC2s, in lung inflammation. *Immunity* 40, 758–771, doi:10.1016/j.immuni.2014.04.013 (2014). [PubMed: 24837103]
15. de Kleer IM et al. Perinatal Activation of the Interleukin-33 Pathway Promotes Type 2 Immunity in the Developing Lung. *Immunity* 45, 1285–1298, doi:10.1016/j.immuni.2016.10.031 (2016). [PubMed: 27939673]
16. Cohen M et al. Lung Single-Cell Signaling Interaction Map Reveals Basophil Role in Macrophage Imprinting. *Cell* 175, 1031–1044.e1018, doi:10.1016/j.cell.2018.09.009 (2018). [PubMed: 30318149]
17. Siracusa MC et al. TSLP promotes interleukin-3-independent basophil haematopoiesis and type 2 inflammation. *Nature* 477, 229–233, doi:10.1038/nature10329 (2011). [PubMed: 21841801]
18. Webb LM et al. The Notch signaling pathway promotes basophil responses during helminth-induced type 2 inflammation. *The Journal of experimental medicine* 216, 1268–1279, doi:10.1084/jem.20180131 (2019). [PubMed: 30975892]
19. Giacomini PR et al. Thymic stromal lymphopoietin-dependent basophils promote Th2 cytokine responses following intestinal helminth infection. *Journal of immunology* 189, 4371–4378, doi:10.4049/jimmunol.1200691 (2012).
20. Ohnmacht C et al. Basophils orchestrate chronic allergic dermatitis and protective immunity against helminths. *Immunity* 33, 364–374, doi:10.1016/j.immuni.2010.08.011 (2010). [PubMed: 20817571]
21. Sullivan BM et al. Genetic analysis of basophil function in vivo. *Nature immunology* 12, 527–535, doi:10.1038/ni.2036 (2011). [PubMed: 21552267]
22. Inclan-Rico JM & Siracusa MC First Responders: Innate Immunity to Helminths. *Trends Parasitol* 34, 861–880, doi:10.1016/j.pt.2018.08.007 (2018). [PubMed: 30177466]
23. Klose CSN et al. The neuropeptide neuromedin U stimulates innate lymphoid cells and type 2 inflammation. *Nature* 549, 282–286, doi:10.1038/nature23676 (2017). [PubMed: 28869965]
24. Cardoso V et al. Neuronal regulation of type 2 innate lymphoid cells via neuromedin U. *Nature* 549, 277–281, doi:10.1038/nature23469 (2017). [PubMed: 28869974]
25. Wallrapp A et al. The neuropeptide NMU amplifies ILC2-driven allergic lung inflammation. *Nature* 549, 351–356, doi:10.1038/nature24029 (2017). [PubMed: 28902842]
26. Wallrapp A et al. Calcitonin Gene-Related Peptide Negatively Regulates Alarmin-Driven Type 2 Innate Lymphoid Cell Responses. *Immunity* 51, 709–723.e706, doi:10.1016/j.immuni.2019.09.005 (2019). [PubMed: 31604686]
27. Nagashima H et al. Neuropeptide CGRP Limits Group 2 Innate Lymphoid Cell Responses and Constrains Type 2 Inflammation. *Immunity* 51, 682–695.e686, doi:10.1016/j.immuni.2019.06.009 (2019). [PubMed: 31353223]
28. Ohki-Hamazaki H Neuromedin B *Progress in neurobiology* 62, 297–312 (2000). [PubMed: 10840151]
29. Gajjar S & Patel BM Neuromedin: An insight into its types, receptors and therapeutic opportunities. *Pharmacological reports : PR* 69, 438–447, doi:10.1016/j.pharep.2017.01.009 (2017).
30. Noti M et al. Thymic stromal lymphopoietin-elicited basophil responses promote eosinophilic esophagitis. *Nature medicine* 19, 1005–1013, doi:10.1038/nm.3281 (2013).
31. Saenz SA, Taylor BC & Artis D Welcome to the neighborhood: epithelial cell-derived cytokines license innate and adaptive immune responses at mucosal sites. *Immunol Rev* 226, 172–190, doi:10.1111/j.1600-065X.2008.00713.x (2008). [PubMed: 19161424]
32. Stegle O, Teichmann SA & Marioni JC Computational and analytical challenges in single-cell transcriptomics. *Nature Reviews Genetics* 16, 133–145, doi:10.1038/nrg3833 (2015).
33. Joseph C et al. Deciphering hematopoietic stem cells in their niches: a critical appraisal of genetic models, lineage tracing, and imaging strategies. *Cell stem cell* 13, 520–533, doi:10.1016/j.stem.2013.10.010 (2013). [PubMed: 24209759]
34. Sutherland TE et al. Chitinase-like proteins promote IL-17-mediated neutrophilia in a tradeoff between nematode killing and host damage. *Nature immunology* 15, 1116–1125, doi:10.1038/ni.3023 (2014). [PubMed: 25326751]

35. Chen F et al. Neutrophils prime a long-lived effector macrophage phenotype that mediates accelerated helminth expulsion. *Nature immunology* 15, 938–946, doi:10.1038/ni.2984 (2014). [PubMed: 25173346]
36. Chen F et al. An essential role for TH2-type responses in limiting acute tissue damage during experimental helminth infection. *Nature medicine* 18, 260–266, doi:10.1038/nm.2628 (2012).
37. Minutti CM et al. A Macrophage-Pericyte Axis Directs Tissue Restoration via Amphiregulin-Induced Transforming Growth Factor Beta Activation. *Immunity* 50, 645–654.e646, doi:10.1016/j.immuni.2019.01.008 (2019). [PubMed: 30770250]
38. Ugajin T et al. FcεRI, but not FcγR, signals induce prostaglandin D2 and E2 production from basophils. *The American journal of pathology* 179, 775–782, doi:10.1016/j.ajpath.2011.04.023 (2011). [PubMed: 21712025]
39. Siracusa MC, Comeau MR & Artis D New insights into basophil biology: initiators, regulators, and effectors of type 2 inflammation. *Ann N Y Acad Sci* 1217, 166–177, doi:10.1111/j.1749-6632.2010.05918.x (2011). [PubMed: 21276006]
40. Monticelli LA et al. Arginase 1 is an innate lymphoid-cell-intrinsic metabolic checkpoint controlling type 2 inflammation. *Nature immunology* 17, 656–665, doi:10.1038/ni.3421 (2016). [PubMed: 27043409]
41. Zhou Y et al. Prostaglandin E(2) Inhibits Group 2 Innate Lymphoid Cell Activation and Allergic Airway Inflammation Through E-Prostanoid 4-Cyclic Adenosine Monophosphate Signaling. *Frontiers in immunology* 9, 501–501, doi:10.3389/fimmu.2018.00501 (2018). [PubMed: 29593738]
42. Shimokawa C et al. Mast Cells Are Crucial for Induction of Group 2 Innate Lymphoid Cells and Clearance of Helminth Infections. *Immunity* 46, 863–874.e864, doi:10.1016/j.immuni.2017.04.017 (2017). [PubMed: 28514691]
43. Roth RL & Levy DA *Nippostrongylus brasiliensis*: peripheral leukocyte responses and correlation of basophils with blood histamine concentration during infection in rats. *Exp Parasitol* 50, 331–341, doi:10.1016/0014-4894(80)90036-3 (1980). [PubMed: 7428910]
44. Ogilvie BM, Hesketh PM & Rose ME *Nippostrongylus brasiliensis*: peripheral blood leucocyte response of rats, with special reference to basophils. *Exp Parasitol* 46, 20–30, doi:10.1016/0014-4894(78)90153-4 (1978). [PubMed: 729690]
45. Loffredo LF et al. Eosinophil accumulation in postnatal lung is specific to the primary septation phase of development. *Scientific Reports* 10, 4425, doi:10.1038/s41598-020-61420-5 (2020). [PubMed: 32157178]
46. Walunas TL et al. CTLA-4 can function as a negative regulator of T cell activation. *Immunity* 1, 405–413, doi:10.1016/1074-7613(94)90071-x (1994). [PubMed: 7882171]
47. Chikuma S et al. PD-1-mediated suppression of IL-2 production induces CD8+ T cell anergy in vivo. *Journal of immunology* 182, 6682–6689, doi:10.4049/jimmunol.0900080 (2009).
48. Klose CS & Artis D Neuronal regulation of innate lymphoid cells. *Curr Opin Immunol* 56, 94–99, doi:10.1016/j.coi.2018.11.002 (2019). [PubMed: 30530300]
49. Nussbaum JC et al. Type 2 innate lymphoid cells control eosinophil homeostasis. *Nature* 502, 245–248, doi:10.1038/nature12526 (2013). [PubMed: 24037376]
50. Flamar A-L et al. Interleukin-33 Induces the Enzyme Tryptophan Hydroxylase 1 to Promote Inflammatory Group 2 Innate Lymphoid Cell-Mediated Immunity. *Immunity* 52, 606–619.e606, doi:10.1016/j.immuni.2020.02.009 (2020). [PubMed: 32160524]

Methods-only references

51. Han H et al. IL-33 promotes gastrointestinal allergy in a TSLP-independent manner. *Mucosal Immunol* 11, 394–403, doi:10.1038/mi.2017.61 (2018). [PubMed: 28656964]
52. Wada T et al. Selective ablation of basophils in mice reveals their nonredundant role in acquired immunity against ticks. *The Journal of clinical investigation* 120, 2867–2875, doi:10.1172/jci42680 (2010). [PubMed: 20664169]

53. Bouchery T et al. The Study of Host Immune Responses Elicited by the Model Murine Hookworms *Nippostrongylus brasiliensis* and *Heligmosomoides polygyrus*. *Current protocols in mouse biology* 7, 236–286, doi:10.1002/cpmo.34 (2017). [PubMed: 29261231]
54. Ohmori K et al. IL-3 induces basophil expansion in vivo by directing granulocyte-monocyte progenitors to differentiate into basophil lineage-restricted progenitors in the bone marrow and by increasing the number of basophil/mast cell progenitors in the spleen. *Journal of immunology* (Baltimore, Md. : 1950) 182, 2835–2841, doi:10.4049/jimmunol.0802870 (2009).
55. Anderson KG et al. Intravascular staining for discrimination of vascular and tissue leukocytes. *Nature protocols* 9, 209–222, doi:10.1038/nprot.2014.005 (2014). [PubMed: 24385150]
56. Jungblut M, Oeltze K, Zehnter I, Hasselmann D & Bosio A Standardized preparation of single-cell suspensions from mouse lung tissue using the gentleMACS Dissociator. *J Vis Exp*, doi:10.3791/1266 (2009).
57. Ewels PA et al. nf-core: Community curated bioinformatics pipelines doi:10.1101/610741 (2019).
58. Liao Y, Smyth GK & Shi W featureCounts: an efficient general purpose program for assigning sequence reads to genomic features. *Bioinformatics* 30, 923–930, doi:10.1093/bioinformatics/btt656 (2014). [PubMed: 24227677]
59. Pertea M et al. StringTie enables improved reconstruction of a transcriptome from RNA-seq reads. *Nat Biotechnol* 33, 290–295, doi:10.1038/nbt.3122 (2015). [PubMed: 25690850]
60. Dobin A et al. STAR: ultrafast universal RNA-seq aligner. *Bioinformatics* 29, 15–21, doi:10.1093/bioinformatics/bts635 (2013). [PubMed: 23104886]
61. Love MI, Huber W & Anders S Moderated estimation of fold change and dispersion for RNA-seq data with DESeq2. *Genome Biol* 15, 550, doi:10.1186/s13059-014-0550-8 (2014). [PubMed: 25516281]
62. Huang da W, Sherman BT & Lempicki RA Systematic and integrative analysis of large gene lists using DAVID bioinformatics resources. *Nature protocols* 4, 44–57, doi:10.1038/nprot.2008.211 (2009). [PubMed: 19131956]

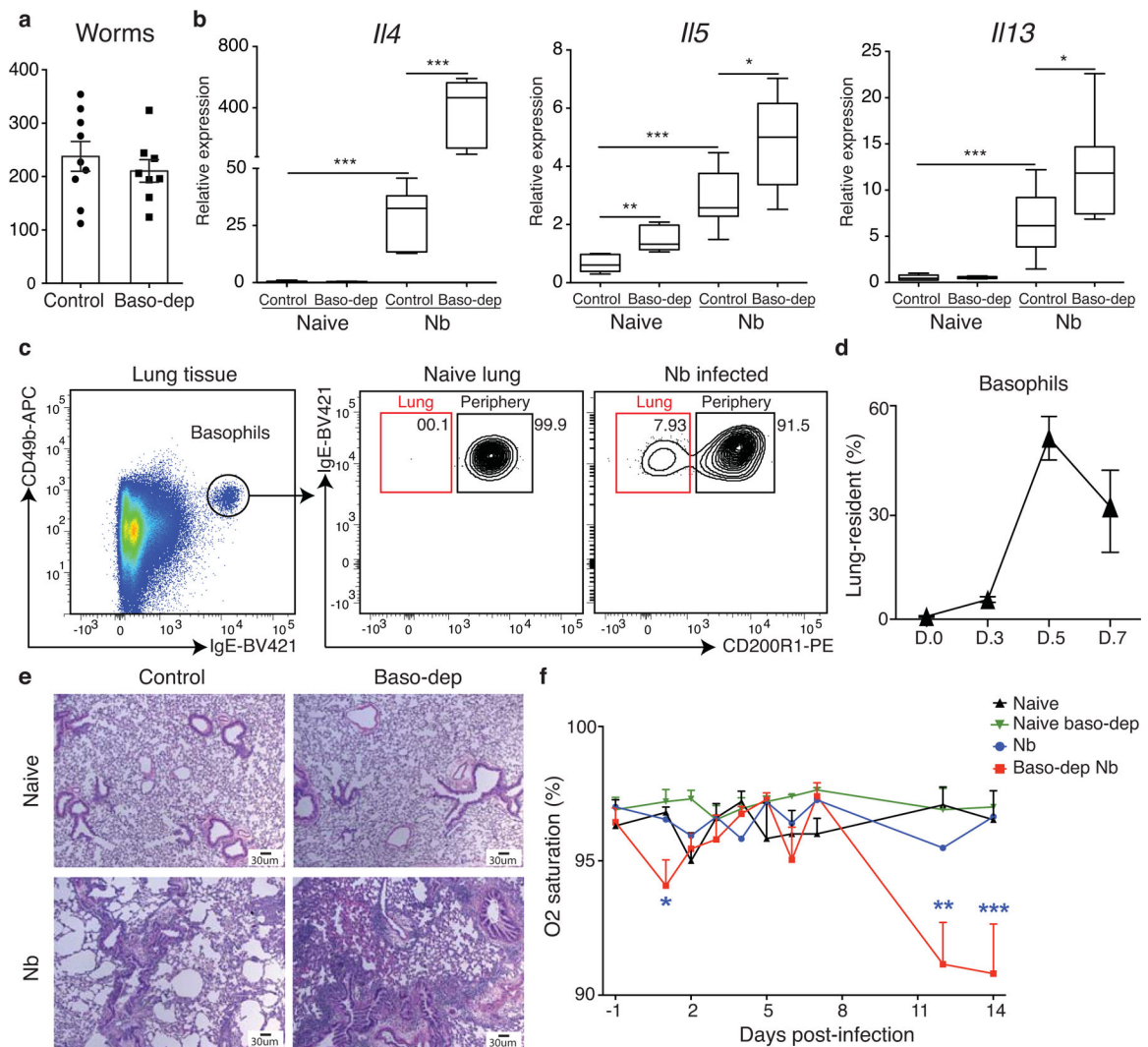
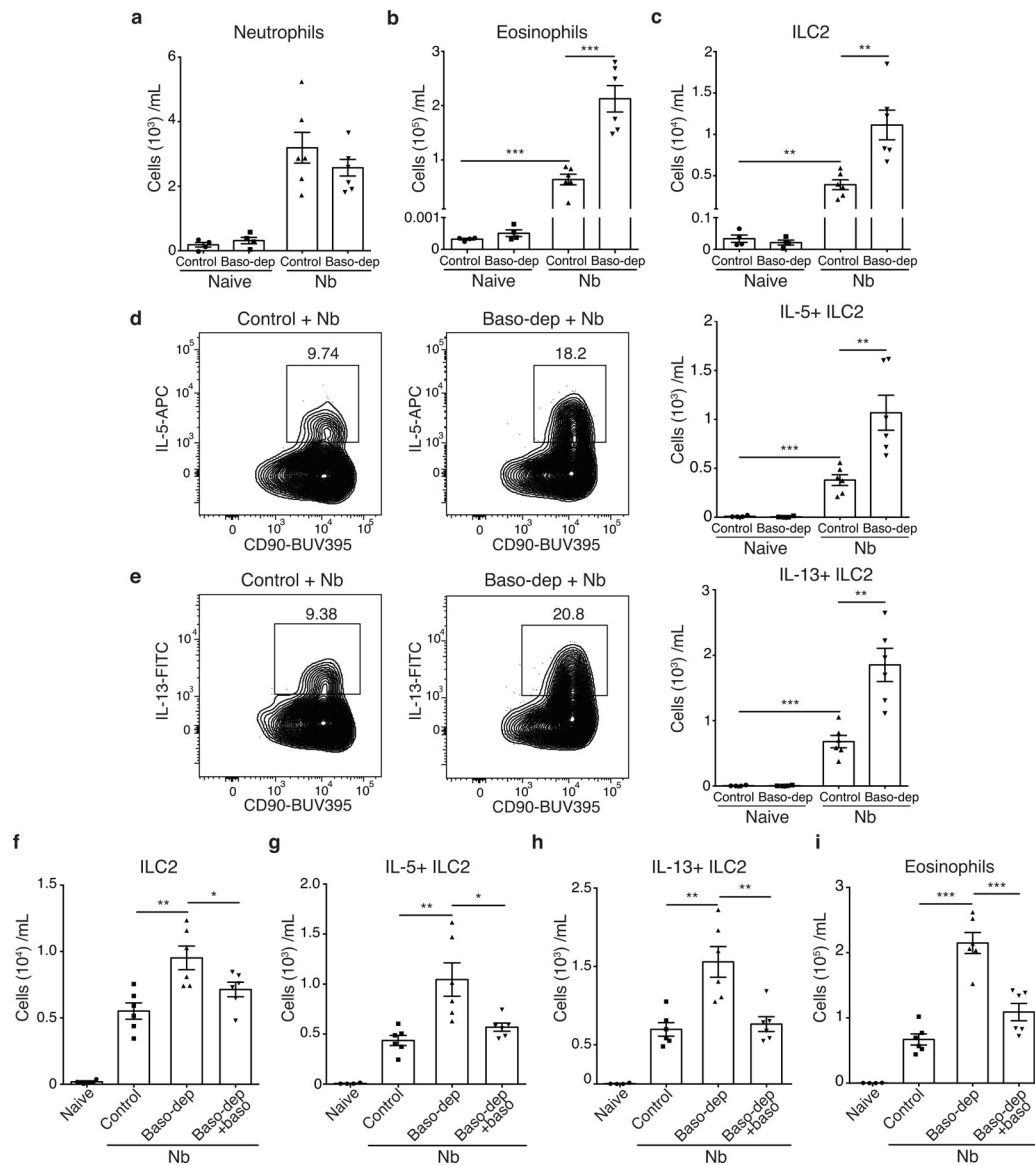


Figure 1. Basophils regulate helminth-induced inflammation.

(a), Intestinal worm burdens were quantified on day 7 post-Nb infection in control or basophil-depleted (baso-dep) mice. (b), Type 2 cytokine expression in the lungs of control and baso-dep mice was determined on day 7 post-Nb infection by real-time PCR. (c), Lung-resident basophils were determined by *in vivo* staining with anti-CD200R1 at day 3 post-infection (d), The percentages of lung-resident basophils were quantified post-Nb infection. (e), Lung pathology was evaluated on day 7 post-Nb infection by hematoxylin and eosin (H&E) staining. (f), Oxygen levels were determined by pulse oximetry for control and baso-dep mice. *P* values were determined by two-tailed Student's *t*-tests. **P* < 0.05, ***P* < 0.01, ****P* < 0.001. (a-f), Representative of at least 3 separate experiments with at least 4 mice per group. (a,b,f), Illustrate data pooled from 2 separate experiments.



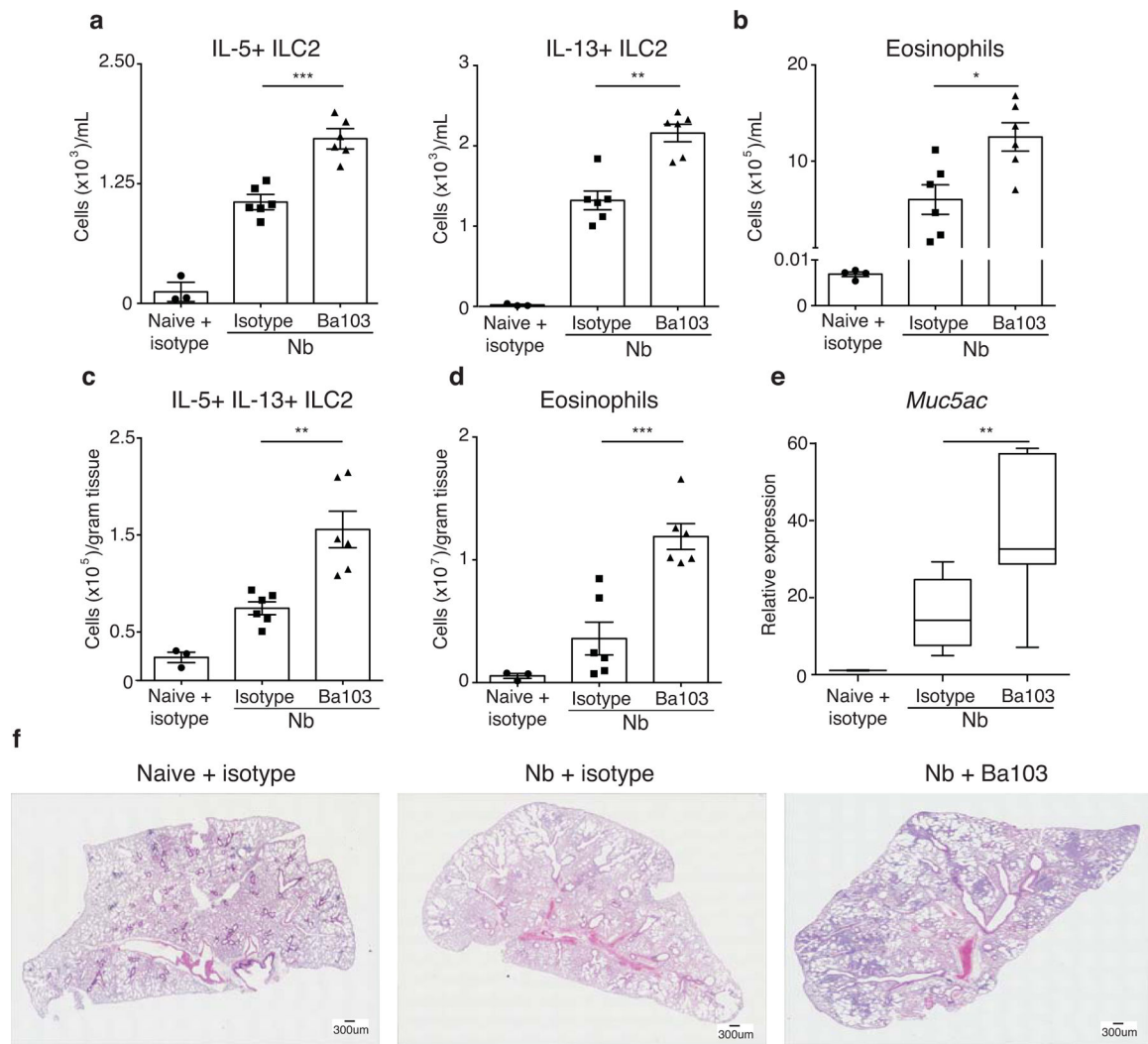


Figure 3. Basophils regulate ILC2 responses independently of T cells.

Nb-infected *Rag2*^{-/-} mice were treated with isotype control or the basophil-depleting antibody Ba103 and (a), IL-5⁺ and IL-13⁺ ILC2s as well as (b), eosinophilia were determined in the BAL and (c, d), lungs on day 7 post-infection. (e), Mucus production in the lung was evaluated by *Muc5ac* expression. (f), H&E staining of lung sections on day 7 post-Nb infection with individual images digitally tiled together to provide a larger overview. *P* values were determined by two-tailed Student's *t*-tests. **P* < 0.05, ***P* < 0.01, ****P* < 0.001. (a-e), Representative of at least 3 separate experiments with at least 2 mice per group. (D), Illustrated data pooled from 2 separate experiments.

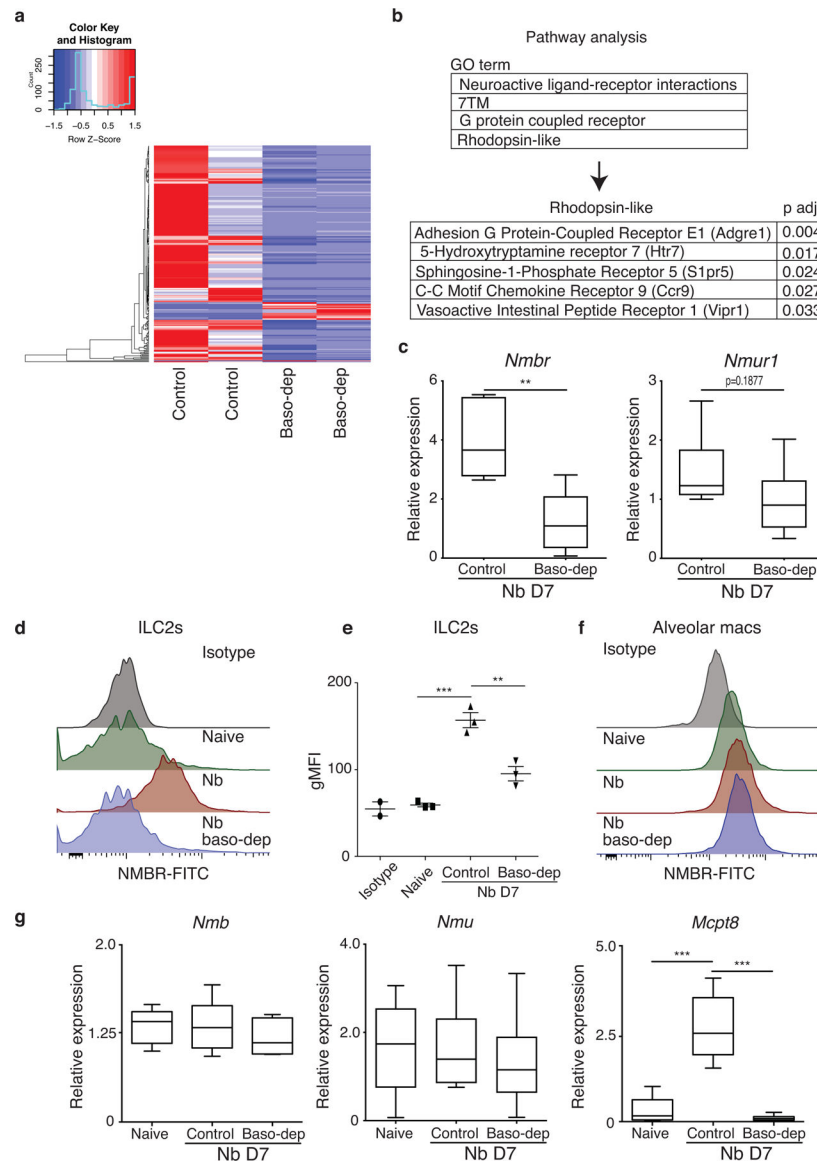


Figure 4. Basophils promote expression of NMBR on ILC2s.

RNA-sequencing analysis of sort-purified ILC2s from the lungs of control or basophil-depleted (baso-dep) mice was performed on day 5 post-Nb. (a), Heat map illustrating genes expressed differently at 2.0-fold or higher between control or baso-dep ILC2s. DAVID pathways analysis of the genes enriched in control ILC2s was performed. (b), Genes enriched in control ILC2s that define the rhodopsin-like pathway. For RT-qPCR studies, lung-resident ILC2s from control or basophil-depleted mice were sort-purified on day 7 post-Nb and (c), *Nmbr* and *Nmur1* expression levels were evaluated. (d), Representative histograms of surface NMBR expression by ILC2s or (f), alveolar macrophages from the lungs of control or baso-dep mice on day 7 post-Nb. (e), gMFI quantification of NMBR expression by ILC2s. (g), *Nmb*, *Nmu*, and *Mcpt8* expression in the lungs of control or baso-dep mice was determined on day 7 post-Nb by real-time PCR. *P* values were determined by two-tailed Student's *t*-tests. **P* < 0.05, ***P* < 0.01, ****P* < 0.001. (c-g), Representative

of at least 3 separate experiments with at least 3 mice per experimental group. (a, b),
Represents data generated from 3 individual samples of ILC2s sort-purified from 5 mice per
experimental group.

Author Manuscript

Author Manuscript

Author Manuscript

Author Manuscript

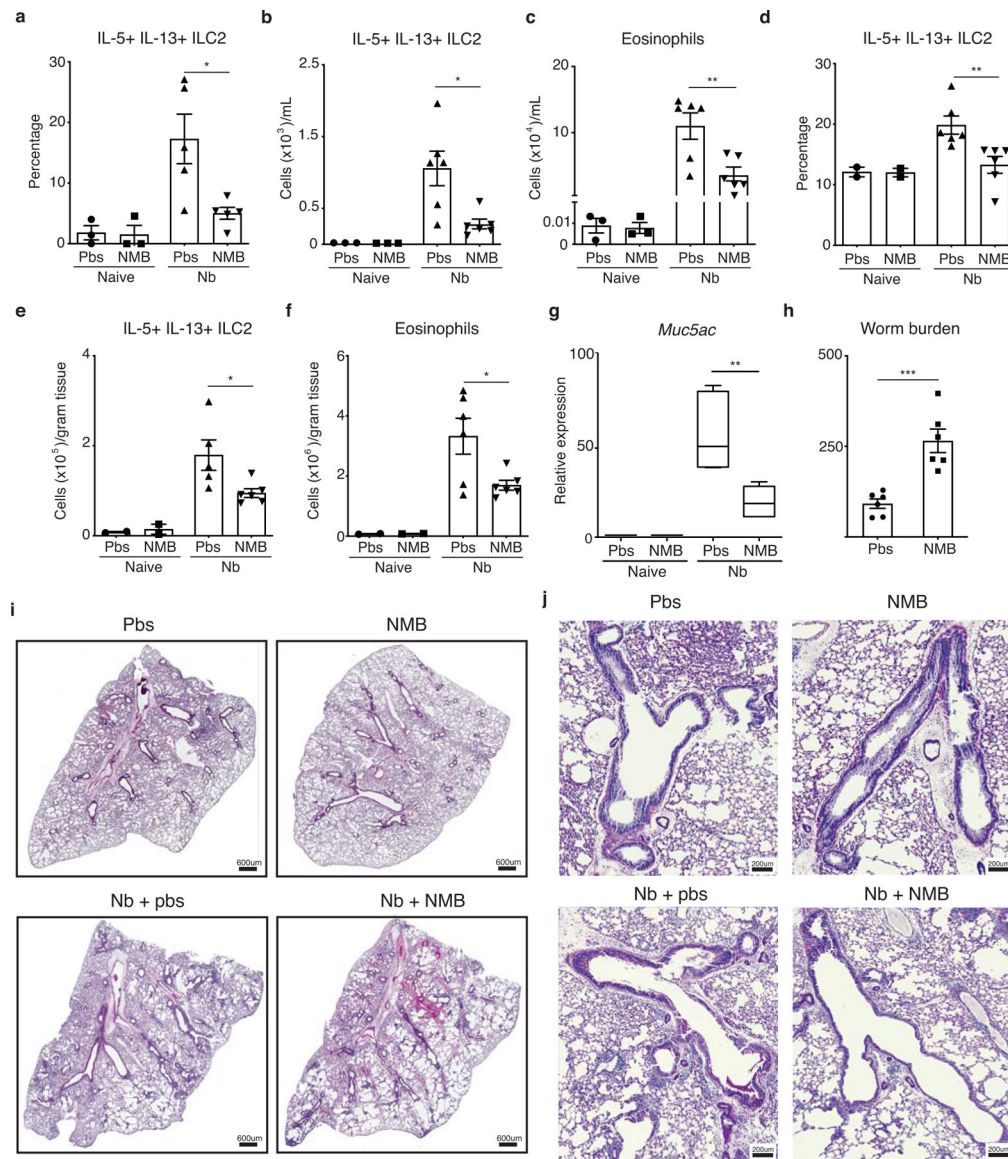


Figure 5. NMB suppresses helminth-induced type 2 cytokine responses.

Nb-infected WT mice were treated daily with PBS or rNMB (i.t.) and (a,b), ILC2 responses and (c), eosinophilia in the BAL were quantified on day 7 post-Nb. (d,e), ILC2 responses, (f), eosinophilia and (g), *Muc5ac* expression were determined in the lungs. (h), Worm burdens were determined in the intestine. (i), Representative lung pathology (H&E staining) and (j), (PAS staining) observed in naïve and Nb-infected mice treated with PBS or rNMB. *P* values were determined by two-tailed Student's *t*-tests. **P* < 0.05, ***P* < 0.01, ****P* < 0.001. (a-j), Representative of at least 2 separate experiments with at least 5 mice per group.

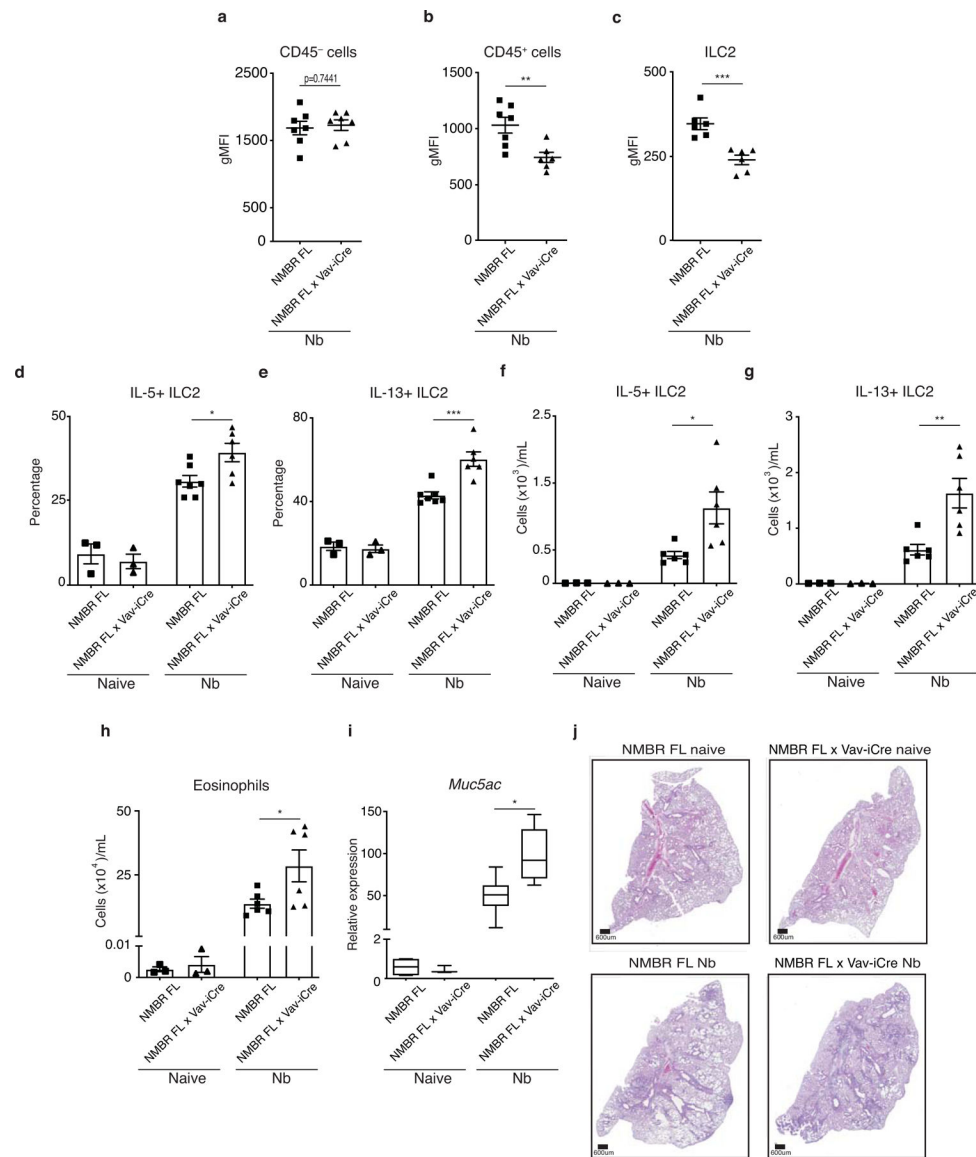


Figure 6. NMBR expression is required to limit helminth-induced inflammation.

NMBR^{fl/fl} mice were generated and crossed with Vav-iCre mice to selectively ablate NMBR expression in hematopoietic cells. Surface expression of NMBR was evaluated in (a), CD45⁻ cells, (b), CD45⁺ cells, and (c), ILC2s of NMBR^{fl/fl} and NMBR^{fl/fl} x Vav-iCre⁺ mice by flow cytometric analysis 7 days post-Nb. (d, f), IL-5⁺ and (e, g) IL-13⁺ ILC2s, as well as (h), eosinophils were quantified in the BAL of NMBR^{fl/fl} x Vav-iCre⁺ mice 7 days post-Nb. (i), RT-qPCR analysis of *Muc5ac* expression and (j), lung pathology (H&E staining) were determined 7 days post-Nb. *P* values were determined by two-tailed Student's *t*-tests. **P* < 0.05, ***P* < 0.01, ****P* < 0.001. (a-j), Representative of at least 3 separate experiments with at least 5 mice per group.

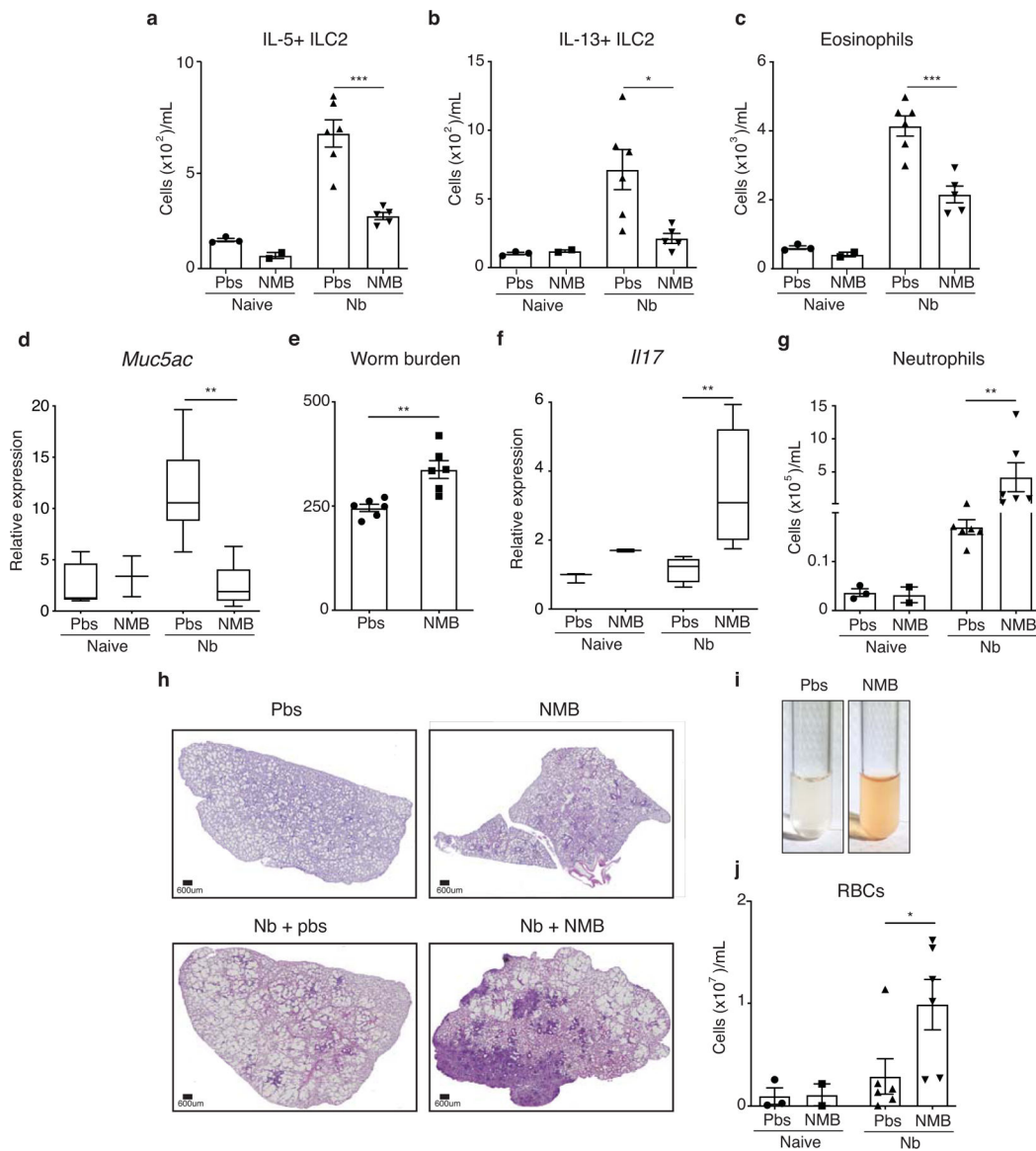


Figure 7. NMB inhibits ILC2-mediated anti-helminth immunity.

Nb-infected *Rag2*^{-/-} mice were treated daily with PBS or rNMB (i.t.) and (a, b) ILC2 responses and (c) eosinophilia in the BAL were quantified 7 days post-Nb infection. (d), *Muc5ac* expression in the lung and (e), worm burdens in the intestine were determined. (f), *Il17* expression and (g), neutrophils in the lungs of *Rag2*^{-/-} mice that were treated with PBS or rNMB (i.t.) following Nb. (h), Lung sections stained with H&E illustrating representative pathology observed in Nb-infected *Rag2*^{-/-} mice were treated with PBS or rNMB. (i), Representative picture illustrating appearance of BAL fluid and (j), quantification of red blood cells in the BAL isolated from Nb-infected *Rag2*^{-/-} mice treated with PBS or rNMB. *P* values were determined by two-tailed Student's *t*-tests. **P* < 0.05, ***P* < 0.01, ****P* < 0.001. (a-j), Representative of at least 3 separate experiments with at least 5 mice per group.

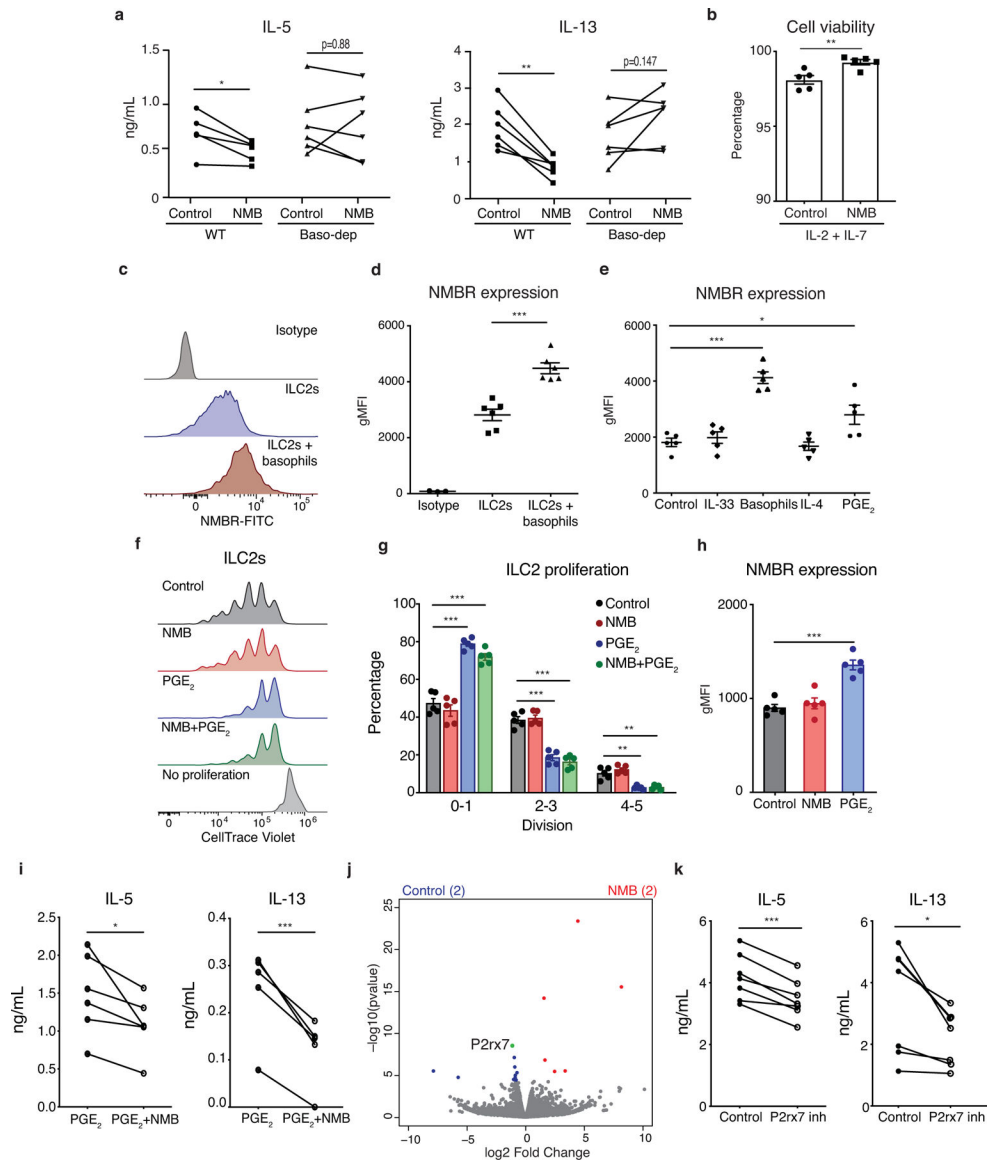


Figure 8. Basophils prime ILC2s for negative regulation by NMB.

ILC2s were sort-purified from the lungs of control or basophil-depleted (baso-dep) mice on day 7 post-Nb and cultured (O/N) with IL-2 and IL-7 in the presence or absence of rNMB. (a), IL-5 and IL-13 levels in culture supernatants were determined by ELISA and (b), cell viability was evaluated by negative staining for 7-AAD and Annexin V. (c), Representative histograms of surface NMBR expression in sort-purified ILC2s cultured (O/N) with IL-2 and IL-7 alone, or with activated basophils. (d), gMFI quantification of NMBR expression by ILC2s. (e), NMBR surface expression was evaluated in sort-purified ILC2s cultured (O/N) with IL-33, basophils, IL-4, and PGE₂ in the presence of IL-2 and IL-7. Sort-purified ILC2s were cultured for 4 days with vehicle, rNMB, PGE₂, or both, in the presence of IL-2 and IL-7 and (f, g), cell proliferation by CTV dilution, (h), surface NMBR expression, and (i), cytokine levels in the supernatant were monitored. (j), Volcano plot of differentially-expressed genes of ILC2s treated with vehicle or rNMB (O/N). (k), Levels of cytokines

in the supernatant of ILC2s cultured (O/N) with vehicle, or in the presence of the P2rx7 inhibitor, brilliant blue G. *P* values were determined by two-tailed Student's *t*-tests. **P* < 0.05, ***P* < 0.01, ****P* < 0.001. (a,b), Representative of 3 separate experiments with at least 5 mice per group. (c-i, k), Representative of 3 separate experiments with data generated from at least 5 individual samples of ILC2s sort-purified from 5 mice per experimental group.

Author Manuscript

Author Manuscript

Author Manuscript

Author Manuscript